CONF-750804--3

HEAT TRANSFER AND FRICTION CORRELATIONS REQUIRED TO DESCRIBE STEAM-WATER BEHAVIOR IN NUCLEAR SAFETY STUDIES*

By

C. W. Solbrig, J. H. McFadden,
R. W. Lyczkowski and E. D. Hughes

ABSTRACT

The description of two-phase flow is important in nuclear safety studies. Recent two-phase flow descriptions are based upon unequal phase velocities and unequal phase temperatures (UVUT) theories with interphase interaction terms. These theories are more mechanistic than homogeneous theories and require more and different types of correlations than homogeneous theories. The UVUT theories require correlations (or models) which describe wall and interphase mass transfer, friction, momentum transfer, and heat transfer for all flow regimes and heat transfer regimes. A set of correlations is presented in this paper which can be used with UVUT theories. These correlations cover the complete range of parameters needed and in all cases are expected to yield reasonable numbers.

* Paper to be presented at the 15th National Heat Transfer conference in the Heat Transfer in Reactor Safety Session, August 10 - 13, 1975, San Francisco, California

TABLE OF CONTENTS

FIGURES

NOMENCLATURE

$\bar{A}_{ab}$	surface area between phases "a" and "b" per unit volume
$\bar{A}_{g\ell}$	surface area between vapor and liquid phases per unit volume
$\bar{A}_{wa}$	surface area of phase "a" in contact with wall per unit volume
$\bar{A}_{wg}$	surface area of vapor phase in contact with wall per unit volume
$\bar{A}_{w\ell}$	surface area of liquid phase in contact with wall per unit volume
$\bar{A}^{q}_{w}$	wall area per unit volume available for heat transfer
$\bar{A}^{q}_{wg}$	wall area per unit volume available for heat transfer between the wall and the vapor phase
$\bar{A}^{q}_{w\ell}$	wall area per unit volume available for heat transfer between the wall and the liquid phase
$\bar{A}^{q}_{g\ell}$	surface area per unit volume available for heat transfer between the vapor and liquid phases
$\bar{A}^{q}_{w\ell,FB}$	wall area per unit volume available for film boiling heat transfer between the wall and the liquid phase
$\bar{A}^{q}_{w\ell,NB}$	wall area per unit volume available for nucleate boiling heat transfer between the wall and the liquid phase
B_{ab}	friction coefficient between phase "a" and phase "b"
$B_{g\ell}$	friction coefficient betwwen vapor and liquid phases
B_{wa}	stationary form and viscous drag between wall and phase "a"
B_{wg}	stationary form and viscous drag between wall and vapor phase
$B_{w\ell}$	stationary form and viscous drag between wall and liquid phase

C_D	drag coefficient for flow over spheres
c_p	specific heat
c_{pa}	specific heat of phase "a"
c_{pg}	specific heat of vapor phase
$c_{p\ell}$	specific heat of liquid phase
D	diameter of control volume
D^a_{hy}	hydraulic diameter of phase "a"
D^a_{int}	interphase hydraulic diameter for phase "a"
D^g_w	hydraulic diameter of vapor phase in contact with wall
D^ℓ_w	hydraulic diameter of liquid phase in contact with wall
F_{ab}	friction force per unit volume exerted on phase "b" by phase "a"
F_{wa}	friction force per unit volume exerted on phase "a" by wall
F_{a3}	fraction of wall heat flux to liquid phase which results in vaporization of liquid
F_{d4}	fraction of heat flux from vapor phase to wall which results in condensation of vapor
F_{e3}	fraction of interphase heat flux which results in vaporization of liquid
F_{e4}	fraction of interphase heat flux which results in condensation of vapor
f	Moody friction factor
f_a	Moody friction factor for phase "a"
f_g	Moody friction factor for vapor phase
f_ℓ	Moody friction factor for liquid phase

G	total mass flux
G_g	mass flux of vapor phase
G_ℓ	mass flux of liquid phase
g	acceleration due to gravity
h	mixture enthalpy
h_ℓ	enthalpy of liquid phase
h_{gs}	enthalpy of saturated vapor
$h_{\ell s}$	enthalpy of saturated liquid
h_{fg}	enthalpy of vaporization
h_C	single phase free or forced convection heat transfer coefficient
$h_{g\ell}$	coefficient for heat transfer between vapor phase and liquid phase
h_w	coefficient for heat transfer between the wall and the fluid
h_{wa}	coefficient for heat transfer between the wall and phase "a"
h_{wg}	coefficient for heat transfer between the wall and the vapor phase
$h_{w\ell}$	coefficient for heat transfer between the wall and the liquid phase
h_{e1}	coefficient for heat transfer between the liquid-vapor interface and the liquid
h_{e7}	coefficient for heat transfer between the liquid-vapor interface and the vapor
k	thermal conductivity
k_a	thermal conductivity of phase "a"
k_g	thermal conductivity of vapor phase
k_ℓ	thermal conductivity of liquid phase

Nu	Nusselt number
P	pressure
P_F	probability of film boiling
P_N	probability of nucleate boiling
Pr	Prandtl number
Pr_g	Prandtl number for vapor phase
Pr_ℓ	Prandtl number for liquid phase
$\dot{q}_w$	heat flux between wall and fluid
$\dot{q}_{CHF}$	critical heat flux
$\dot{q}_{g\ell}$	heat flux between vapor phase and liquid phase
$\dot{q}_{e1}$	heat flux between liquid-vapor interface and liquid phase
$\dot{q}_{e7}$	heat flux between liquid-vapor interface and vapor phase
q_w	wall heat transfer rate per unit volume
$q_{g\ell}$	interphase heat transfer rate per unit volume
$q_{w\ell}$	heat transfer rate between wall and liquid phase per unit volume
q_{wg}	heat transfer rate between wall and vapor phase per unit volume
q_{a1}	heat transfer rate between wall and liquid phase per unit volume which heats the liquid
q_{a3}	heat transfer rate between wall and liquid phase per unit volume which vaporizes liquid
q_{d4}	heat transfer rate between vapor phase and the wall per unit volume which condenses vapor
q_{d7}	heat transfer rate between vapor phase and wall per unit volume which cools the vapor

q_{e1}	interphase heat transfer rate per unit volume which heats the liquid
q_{e3}	interphase heat transfer rate per unit volume which vaporizes liquid
q_{e4}	interphase heat transfer rate per unit volume which condenses vapor
q_{e7}	interphase heat transfer rate per unit volume which cools the vapor
R	radius of control volume
R_i	radius of inner core in annular or inverse annular flow
Re	Reynolds number
Re^a_{int}	interphase Reynolds number for phase "a"
Re^a_w	Reynolds number for phase "a" for wall terms
Re_p	particle Reynolds number
r_p	mean radius for bubble or drop
T	temperature
T_a	temperature of phase "a"
T_f	film temperature
T_g	temperature of vapor phase
T_ℓ	temperature of liquid phase
T_s	saturation temperature
T_w	wall temperature
T_{CHF}	wall temperature at point of critical heat flux

V_C	control volume
V_{sg}	superficial vapor phase velocity
$V_{s\ell}$	superficial liquid phase velocity
v	velocity
v^a	velocity of phase "a"
v^g	velocity of vapor phase
v^ℓ	velocity of liquid phase
$\bar{v}_r$	molecular velocity
We_{crit}	critical Weber number
x	thermodynamic quality
α	vapor volume fraction
δ	film thickness
δ_g	film thickness of vapor phase
δ_ℓ	film thickness of liquid phase
ε	pipe roughness
ε_o	Reynolds flux
θ	angle subtending chord along liquid surface in separated horizontal flow
μ	viscosity
μ_g	viscosity of vapor phase

μ_ℓ	viscosity of liquid phase
μ_W	viscosity of water at standard conditions
ρ	density
ρ_a	density of phase "a"
ρ_A	density of air at standard conditions
ρ_c	density of continuous phase
ρ_g	density of vapor phase
ρ_ℓ	density of liquid phase
ρ_W	density of water at standard conditions
ρ_{gs}	density of vapor phase at saturation pressure
$\rho_{\ell s}$	density of liquid phase at saturation pressure
σ	surface tension
σ_W	surface tension for air-water at standard conditions

1. INTRODUCTION

The description of two phase flow is important in the analysis of the loss-of-coolant accident as well as in the analysis of many important industrial processes. Recent approaches have included the description of two phase flow with two sets of transport equations, one for the liquid and one for the vapor. The class of theories which use two equation sets to describe unequal phase velocity and unequal phase temperature but assume equal phase pressures will be referred to herein as UVUT theories. Examples of such theories are given by Bouré et al (1971) and Harlow and Amsden (1974). These theories are more mechanistic than equal velocity, equal temperature (EVET) theories and consequently require more and different type of correlations than EVET theories. The purpose of this paper is to present a complete set of correlations which can be used with UVUT theories to close these equation sets. In particular, these correlations have been used in the SSUVUT [a] and SLOOP [a] computer programs. These programs describe one-dimensional flow, the first being steady state and the second being transient. Both of these programs are based upon UVUT theories. The UVUT theories require correlations (or models) which describe wall and interphase mass transfer, friction, momentum transfer, and heat transfer. These correlations are dependent on the geometry of the flow regime present and, thus, models for the flow regimes must be included. Correlations (or models) are presented in this paper to describe the following:

1) flow regime
2) friction force
3) intrinsic velocity
4) heat transfer regime and CHF correlations
5) heat transfer correlations
6) energy partition functions.

---

[a] Computer programs developed by Aerojet Nuclear Company

Flow regime maps are used primarily to determine which friction models are selected. Flow regimes are also used in the determination of heat transfer regimes. In some cases, such as dispersed flow, the heat transfer regimes determine the flow regime. The intrinsic velocity model currently used in the calculation of interphase momentum transfer is the same for all flow regimes. Energy partition functions are used to determine the fraction of heat transferred which goes into nonequilibrium effects, such as subcooled boiling.

2. FLOW REGIME MAPS

The source terms in the UVUT equations are flow regime dependent, so that proper evaluation of these terms (in particular the friction terms) requires that the flow regime in the control volume be known. The flow regime in general is a function of the phase velocities, densities, and viscosities, the vapor fraction, the flow direction, the heat flux to the fluid, interphase heat transfer, the geometry of the confining walls, and transient and convective momentum and energy effects. The published flow regime maps do not take into account all of these variables. In fact, the published flow regime maps are usually for cocurrent upward flow or horizontal, one-dimensional, steady state, isothermal flow. Some limited experimental results and analytical models (Wallis, 1969) have been presented for countercurrent flow. Although the model presented here is based on published steady state flow regime maps, simple analytical models can be used to predict flow regime transitions. Kordyban and Ranov (1970), for example, have presented a model for the transition between stratified and slug flows which agrees well with experimental data. Govier and Aziz (1972, p. 389) have presented a model for transition between bubble and slug flows. Transient and convective effects can be included through use of analytical models. Future versions of these flow regime maps are intended to include these effects. The flow regime maps which are used are based on those presented in the literature by Bennett et al. (1965) for vertical flow and Baker (1954) for horizontal flow. These maps have been modified in a simple manner to include the effects of heat transfer and countercurrent flow. Three-dimensional effects have not been accounted for but three-dimensional flows with many imbedded stationary surfaces can probably be accounted for with appropriate modifications of the flow regime maps presented here.

2.1 Geometry of the Flow Regimes Considered

The flow regimes considered in the present UVUT correlation model are described in in this section.

2.1.1 Single Phase. Single phase fluid is assumed if the vapor volume fraction α is zero (all liquid) or unity (all vapor).

2.1.2 Annular and Inverse Annular Flow. Annular flow is viewed as one phase flowing in the central cylindrical region of a cylindrical pipe with the other phase flowing in the annulus formed by the central cylindrical region and the pipe walls. Normal annular flow has vapor in the center region and water on the wall. Inverse annular flow has water in the center region and vapor on the wall. Presumably, inverse annular flow can only occur in the presence of a hot wall which would prohibit liquid from staying on the wall. Annular flow in noncylindrical geometries could be represented with effective hydraulic diameters. In three-dimensional geometries, the concept of annular flow may become indistinguishable from stratified flow or inverse annular flow. The major differences in flow regimes may be whether the two phases are each essentially contiguous or whether one of them is dispersed in the other. Differences calculated in the friction forces between annular and stratified flows may be inconsequential when UVUT theory is applied, but remains to be confirmed.

2.1.3 Dispersed Flow (Also known as Mist or Droplet Flow). Dispersed flow as used here refers to a flow pattern in which liquid droplets are dispersed in a continuous gas phase. In adiabatic systems, an increase in the vapor flow rate for annular flow causes the liquid film flow to become turbulent. A further increase in the vapor flow increases the entrainment rate, with the liquid film eventually

breaking up completely. If an external heat source is present, dispersed flow is also possible in the transition and stable film boiling heat transfer regimes. When a heat source is present, the transition from dispersed flow to inverse annular flow is assumed to depend on the volume fraction of vapor. If the vapor volume fraction is less than 0.2, inverse annular flow is assumed.

2.1.4 Countercurrent Flow. If the velocities of both phase are of opposite sign, annular flow is assumed. Inverse annular flow is assumed (vapor on the wall, liquid center core) if the wall temperature, T_w, is greater than or equal to the wall temperature which corresponds to critical heat flux, T_{CHF}. Normal annular flow (liquid on wall, vapor center core) is assumed if the wall temperature is less than T_{CHF}.

2.1.5 Stagnation. Stagnation is specified as both phases being stagnant. A total mass flux of zero with the phases moving in the opposite direction qualifies as countercurrent flow. Stagnation in a horizontal pipe is different than in a vertical pipe. Stagnation in a horizontal pipe is viewed as a completely separated geometry with liquid on the bottom and vapor on the top. Such stagnation is consistent with the Baker (1954) regime map for horizontal flow and low velocity. Stagnation in a vertical pipe is viewed as a uniform distribution of bubbles in the liquid phase.

2.1.6 Bubble Flow. This flow regime assumes that bubbles are uniformly distributed in a continuous liquid phase. The bubble phase is in contact with the wall. The area of each phase in contact with the wall is assumed to be proportional to the corresponding volume fractions.

2.1.7 Slug Flow (Plug Flow). Slug flow is viewed as a regime with the wall covered with liquid. The gas phase is distributed as large elongated slugs in a continuous liquid. This regime is approximated as annular flow for the purpose of computing interfacial friction and interphase heat transfer.

2.1.8 Froth Flow (Churn Flow). Froth flow occurs when the phase velocity difference is too great to support slug flow but not large enough to give annular flow. The flow is turbulent with the vapor bubbles having irregular shapes. This regime is approximated as bubble flow.

2.1.9 Stratified Flow. Stratified flow is considered only in horizontal pipes. The flow is assumed to be completely separated with liquid on the bottom and vapor on the top.

2.1.10 Flow Regimes Not Explicitly Considered. Annular dispersed flow is a flow regime with a liquid film on the wall and gas center region with droplets distributed in the gas phase. This flow regime occurs during the transition from annular to dispersed flow. (Govier and Aziz, 1972, p 416). This regime is inconsistent with the two component UVUT theories since three velocities are required to describe the flow: 1) the liquid film; 2) the gas core; and 3) the liquid droplets. This regime is approximated here as annular flow with all the liquid assumed to be in the wall film. Studies (Farman and McFadden, 1974) have shown that in steady state this assumption is adequate.

Wispy Annular flow (Bennett et al., 1965) is similar to annular dispersed flow, except that the liquid fraction entrained is less than in annular dispersed flow, and the liquid is entrained as large agglomerates as opposed to small droplets. The region identified as wispy-annular on Bennett's map is treated as annular flow here.

For horizontal flow, Baker (1954) and Govier (1972) include two flow regimes which have been combined here with other flow regimes. These regimes are wave flow and elongated bubble (plug) flow. Wave flow is combined with separated flow because both are similar. An effective interface roughness is used in the separated flow model which is due to surface waves so that, in effect, both of these regimes are assumed to have waves. Elongated bubble is combined with slug flow. Both of these regimes are transitions between bubble and separated flow, so that the differences between these flow regimes are assumed to be insignificant.

One flow regime which should be included in future refinements is separated vertical flow. This regime can occur between two heated walls when one is dry and the other wetted.

Most of the flow regimes discussed in this section can occur in flow in an inclined pipe as well as in a vertical or horizontal pipe. In the UVUT code, all inclined pipes are treated as vertical pipes for the purpose of determining flow regimes.

2.2 Method of Flow Regime Selection

The method used to select the flow regime is shown in Figure (2.i). If the fluid is single phase, the determination is complete. The fluid is next checked for countercurrent flow which automatically puts the fluid in one of the two

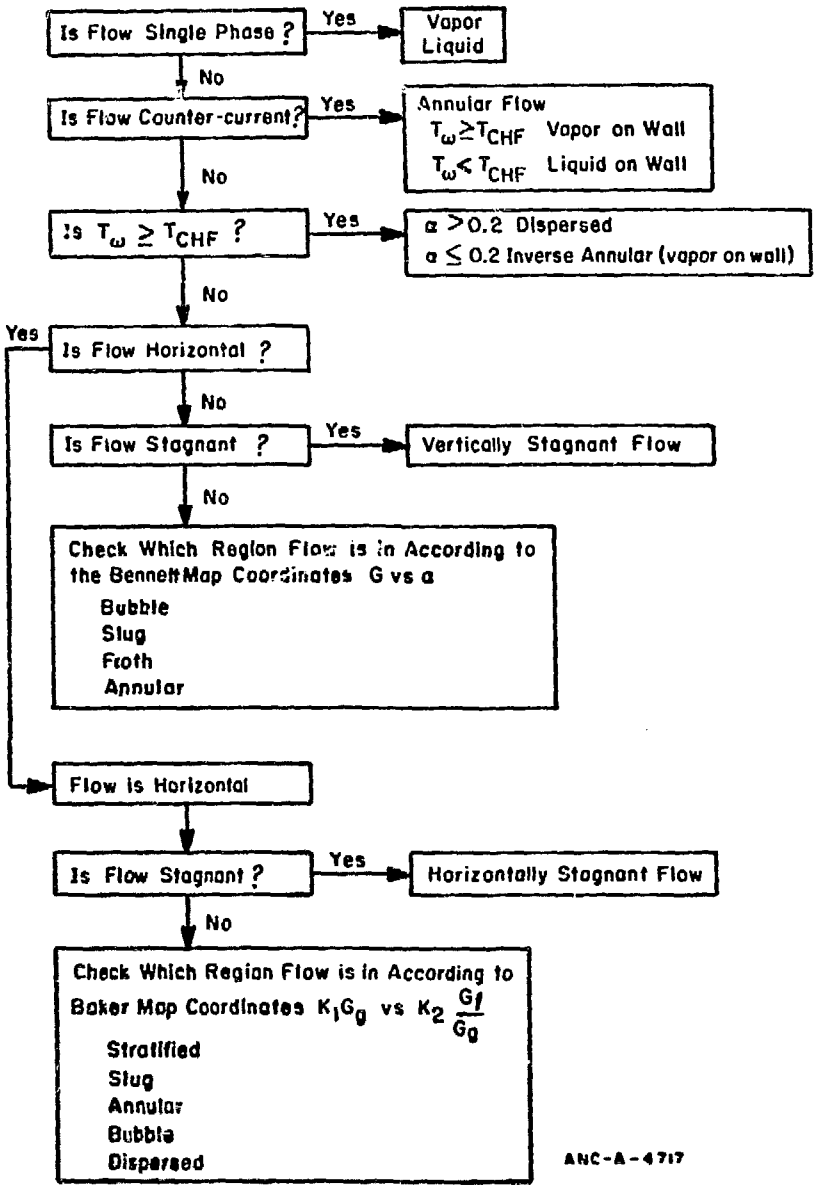

Figure 2.1 Flow Regime Selection Logic

annular flow regimes. Next, the critical heat flux condition is checked. If the wall temperature is greater than the temperature corresponding to critical heat flux, T_{CHF}, then no liquid exists on the wall so that the flow is either dispersed or inverse annular. The method of determining T_{CHF} is described in Section 6.3 The orientation of the pipe is next determined. If it is vertical or inclined, the Bennett (1956) flow regime map is used unless the flow is stagnant. Stagnation is assumed if the total mass flow is less than $1x10^4$ lbm/ft^2-hr. If the flow is horizontal, the Baker (1954) flow regime map is used unless the flow is stagnant. Again, stagnation is assumed if the total mass flow is less than $1x10^4$ lbm/ft^2-hr. These two flow regime maps are described in the following sections.

This selection of flow regime would have to be extended to better describe flow in inclined pipes and three dimensional flows.

2.3 Bennett Flow Regime Map for Vertical Flow

Bennett's flow regime map (Bennett, et al., 1965) is based on visual studies of water-steam flowing upward in a vertical tube. Bennett plotted the results using the coordinates of the total mass flux, G, versus the thermodynamic quality, x, defined as

$$G = \alpha\rho_g v^g + (1-\alpha)\rho_\ell v^\ell \tag{2.1}$$

where

α = volume fraction of steam,

ρ_a = thermodynamic density of phase "a"

v^a = velocity of phase "a".

$$x = \frac{h - h_{\ell s}}{h_{fg}} \tag{2.2}$$

where h = mixture enthalpy,

$h_{\ell s}$ = saturation enthalpy of the liquid at the mixture pressure, and

h_{fg} = enthalpy of vaporization at mixture pressure.

Figure (2.2) represents data obtained at 1000 psia in a 0.5-inch-ID circular conduit. Bennett's map is believed to be more independent of pressure if the thermodynamic quality "x" is converted to the volume fraction, α. The relation between quality and α is a unique expression at constant pressure and for the range $0 \leq x \leq 1$ is given by

$$\alpha = \frac{\frac{x}{\rho_{gs}}}{\frac{(1-x)}{\rho_{\ell s}} + \frac{x}{\rho_{gs}}} \qquad (2.3)$$

where ρ_{as} = thermodynamic density of phase "a" at saturation pressure

The original regime map by Bennett (1965) is shown in Figure (2.2), and the modified flow regime map is shown in Figure (2.3). The flow regime boundaries have been approximated by straight lines in Figure (2.3). The map shown in Figure (2.3) is assumed to be valid for vertical cocurrent upflow and downflow. The flow regime boundary between annular and bubble flows is maintained at $\alpha = 0.24$ for mass fluxes above 3×10^6 lbm/ft^2-hr even though data are not reported beyond this value by Bennett. The upper boundary of annular and wispy annular flow in Figure (2.2) separates those regions from post CHF conditions. In Figure (2.3), these two regions are treated as annular flow except when CHF is exceeded, as mentioned previously, in which case they are treated as post CHF flow.

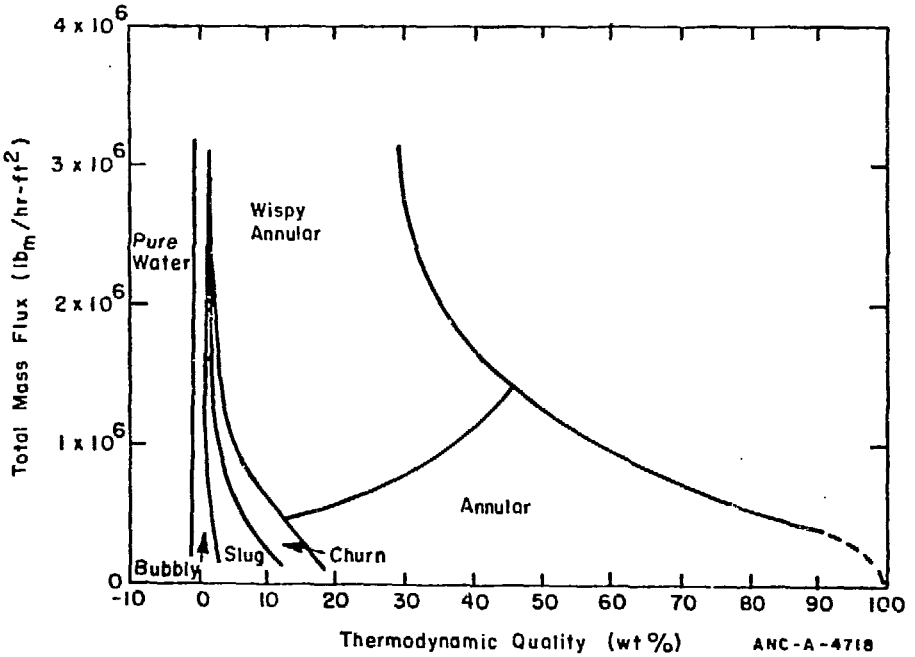

Figure 2.2 Results of Bennet et al. (1965) for Flow Patterns Produced by Boiling in a 1/2-in. Bore Tube at 1000 psia

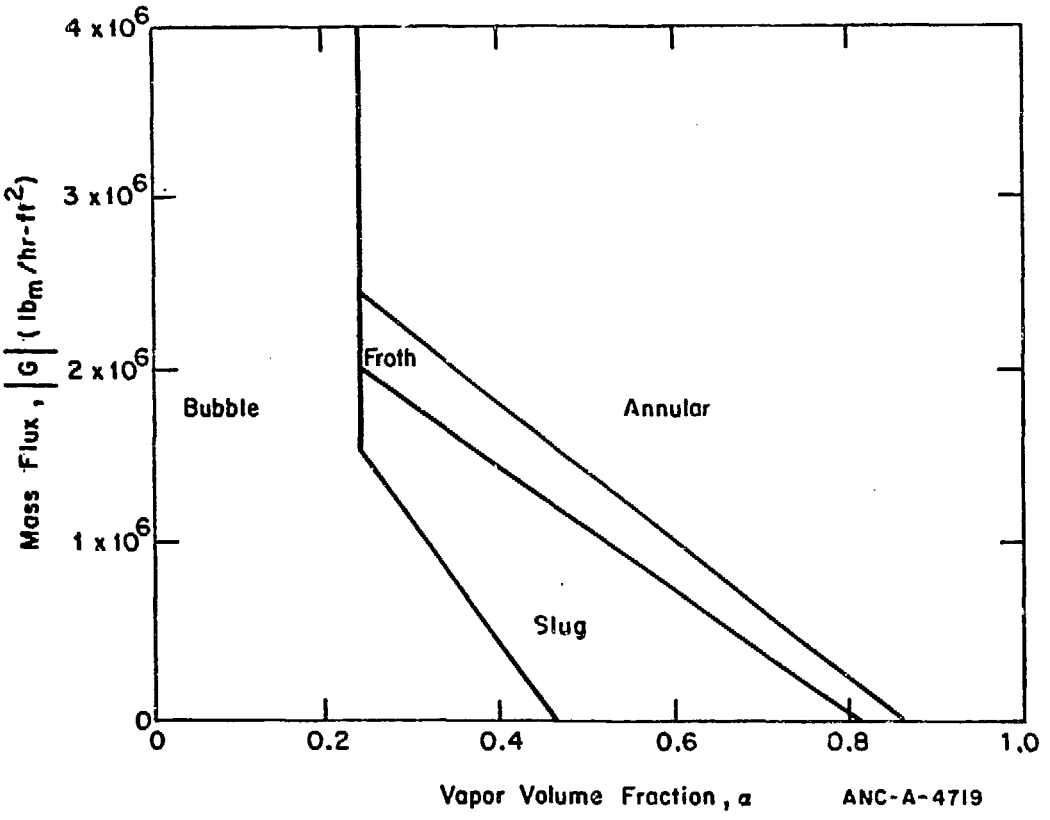

Figure 2.3 Flow Regime Map for Vertical Flow

2.4 Baker Flow Regime Map for Horizontal Flow

The flow regime map of Baker (1954), shown in Figure (2.4), is used as a basis for determining flow regimes for horizontal flow. Scott (1963, p 209) pointed out that the flow regime boundaries are independent of tube diameter for tube sizes greater than one inch (based on gas-oil data) but that these regime boundaries will tend to change rapidly as diameters decrease below one inch.

The coordinates of the Baker map are dependent on the mass velocity of the vapor, G_g, (ordinate) and the ratio of the liquid mass velocity, G_ℓ, to the vapor mass velocity (abcissa). The coordinates are

$$\frac{G_g}{\lambda} \quad \text{and} \quad \frac{G_\ell \, \lambda \psi}{G_g} \tag{2.4}$$

where

$$G_g = \alpha \rho_g v^g \tag{2.5}$$

$$G_\ell = (1-\alpha) \, \rho_\ell \, v^\ell \tag{2.6}$$

$$\lambda = \left[\left(\frac{\rho_g}{\rho_A} \right) \left(\frac{\rho_\ell}{\rho_W} \right) \right]^{\frac{1}{2}} \tag{2.7}$$

$$\psi = \left(\frac{\sigma_W}{\sigma} \right) \left[\left(\frac{\mu_\ell}{\mu_W} \right) \left(\frac{\rho_W}{\rho_\ell} \right)^2 \right]^{1/3} \tag{2.8}$$

σ = surface tension

μ = absolute viscosity.

Subscripts "A" and "W" refer to air and water properties evaluated at standard atmospheric conditions of 60°F and 14.65 psia. [$\rho_A = 0.075$ lbm/ft^3, $\rho_W = 62.3$ lbm/ft^3, $\sigma_W = 73$ dynes/cm, $\mu_W = 1$ centipoise (Baker, 1954)].

Approximations made to facilitate coding of the Baker map are:

(1) Wavy and stratified flow are grouped as stratified (separated) flow.

(2) The plug flow regime is grouped with the slug flow regime.

(3) The flow regime boundaries were linearized in log-log coordinates.

The modified Baker map is given in Figure (2.5).

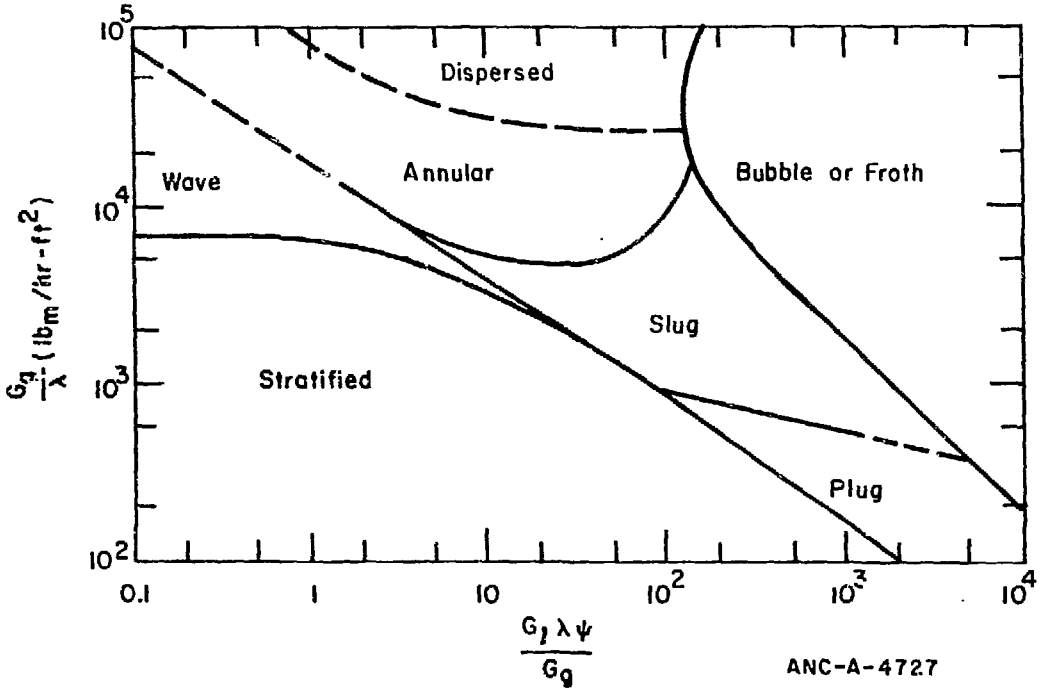

Figure 2.4 Flow Pattern Diagram for Horizontal Flow (Baker, 1954)

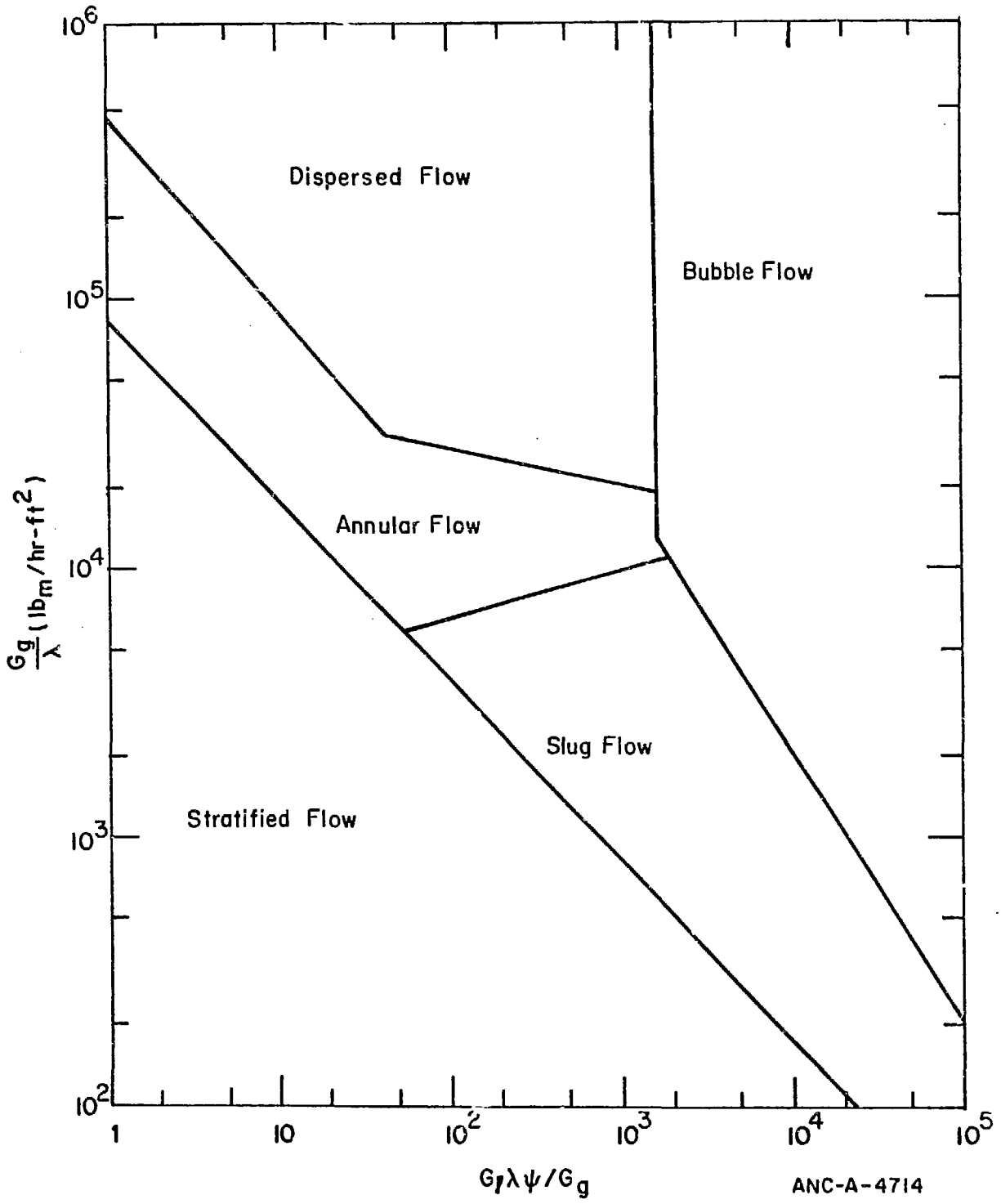

Figure 2.5 Modified Baker Horizontal Flow Regime Map

2.5 Alternate Regime Maps (Govier, 1972)

An alternate set of flow regime maps is available from Govier (1972) and is based on cocurrent air-water flow in a tube.

The coordinates for Govier's horizontal flow map are superficial velocities,

$$V_{s\ell} = (1-\alpha)\, v^{\ell} \tag{2.9}$$

$$V_{sg} = \alpha v^{g}. \tag{2.10}$$

As on the Baker map, stratified and wavy flow have been combined as stratified (separated) flow, and elongated bubble and slug flows have been combined as slug flow. The map as modified here is given in Figure (2.6).

The vertical flow regime map has modified superficial velocities as coordinates, given by

$$YV_{s\ell} \text{ and } XV_{sg} \tag{2.11}$$

where

$$Y = \left[\left(\frac{\rho_{\ell}}{\rho_W}\right)\left(\frac{\sigma_W}{\sigma}\right)\right]^{1/4} \tag{2.12}$$

and

$$X = \left(\frac{\rho_g}{\rho_A}\right)^{1/3} Y. \tag{2.13}$$

Subscripts "W" and "A" mean water and air properties, respectively, and standard atmospheric conditions. A modified Govier flow regime map for vertical flow is shown in Figure (2.7). On this map, the flow regime boundaries are approximated as straight lines.

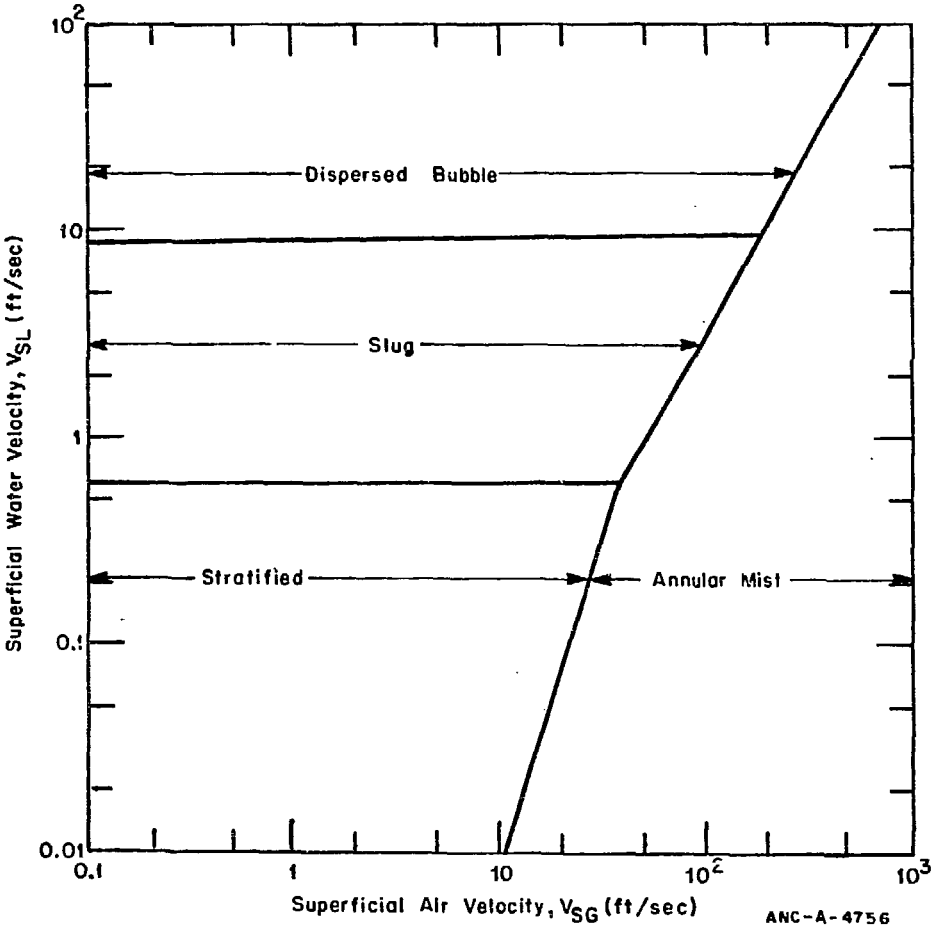

Figure 2.6 Modified Horizontal Flow Map

(Govier, 1972)

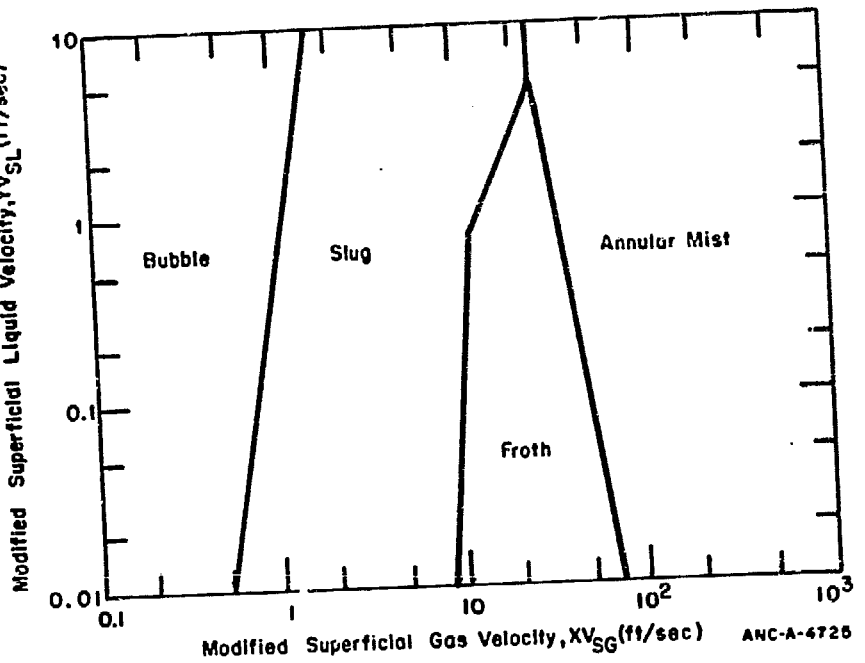

Figure 2.7 Modified Vertical Flow Map (Govier, 1972)

2.6 Summary of Flow Regimes

The flow regimes which are used to compute flow regime dependent terms are summarized. In all cases (unless noted differently), the vapor fraction ranges from 0 to 1, and T_w is less than T_{CHF} (T_{CHF} is defined in Section 6.3)

1) Single phase liquid $\alpha = 0$
2) Bubble
3) Slug
4) Froth (churn)
5) Annular (liquid on wall)
6) Single phase vapor $\alpha = 1$
7) Dispersed $0.2 \leq x < 1$, $T_w > T_{CHF}$
8) Inverse annular (vapor wall) $0 < \alpha < 0.2$, $T_w > T_{CHF}$
9) Stagnation (vertical)
10) Separated
11) Countercurrent (liquid on surface)
12) Countercurrent (vapor on surface), $T_w > T_{CHF}$
13) Stagnation (horizontal)

3. FRICTION FORCES

The flow regime maps are used primarily to determine the correct expression to be used for calculating friction. In the UVUT equations, two types of friction forces are considered.

The first is the friction force per unit volume, F_{wa}, exerted on phase "a" by a stationary surface,

$$F_{wa} = -\bar{A}_{wa} B_{wa} v^a \tag{3.1}$$

where

$\bar{A}_{wa}$ = surface area of phase "a" in contact with the wall per unit volume[a]

B_{wa} = stationary surface form and viscous drag.

The second type of friction force F_{ab} is due to interphase friction, and is given by

$$F_{ab} = -\bar{A}_{ab} B_{ab} (v^a - v^b) \tag{3.2}$$

where

$\bar{A}_{ab}$ = surface area between phases "a" and "b" per unit volume

B_{ab} = friction coefficient between phase "a" and phase "b".

---

[a] The volume referred to throughout this work is the volume available to fluid flow. It does not include the volume of any imbedded objects such as fuel rods. Therefore, all the velocities used are absolute velocities.

For interphase terms the assumptions are

$$\bar{A}_{ab} = \bar{A}_{ba} \tag{3.3}$$

and

$$B_{ab} = B_{ba} \tag{3.4}$$

so that

$$F_{ab} = F_{ba} .$$

In order to compute the terms in Equations (3.1) and (3.2), the phase hydraulic diameter D^a_{hy}, and for dispersed flow, the particle size, r_p, must be known. Correlations for $\bar{A}_{wa}$, B_{wa}, $\bar{A}_{ab}$, B_{ab}, D^a_{hy}, and r_p (for dispersed flow) will be presented in this section for all flow regimes (Section 3.). Where geometrical assumptions involving the system boundaries are required, one dimensional flow in a pipe is assumed. Modifications are expected to be required for other confining geometries but the pipe geometry is expected to be representative of all geometries. The control volume for all flow regimes is taken as a cylinder of radius R and length Δx and is given by

$$V_c = \pi R^2 \Delta x . \tag{3.5}$$

The geometrical representations for annular flow and separated flow are given in Figures (3.1) and (3.2), respectively. For other types of two phase flow, such as bubble, froth and dispersed drops, the dispersed phase is assumed to be made up of uniform size droplets or bubbles uniformly distributed in the continuous phase.

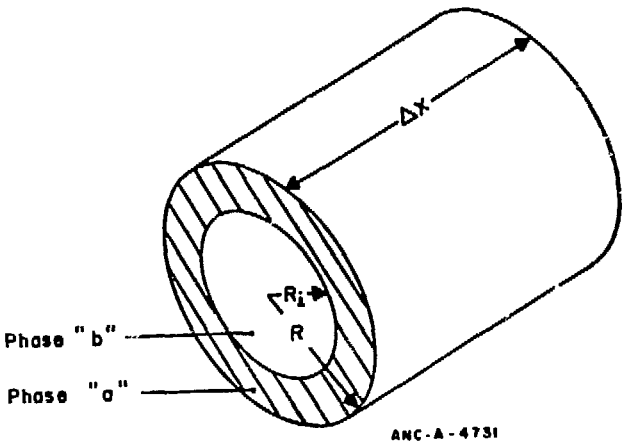

Figure 3.1 Assumed Annular Flow Geometry

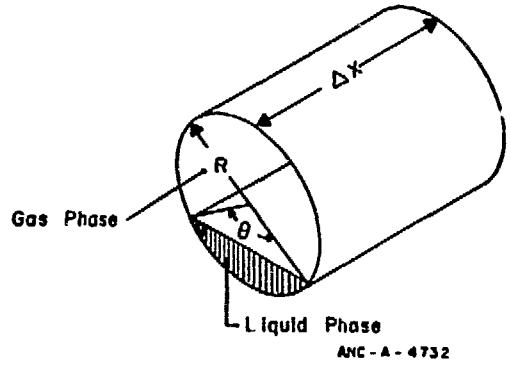

Figure 3.2 Assumed Separated Flow Geometry

3.1 Phase Surface Area in Contact With Wall Per Unit Volume

The phase surface area in contact with the wall per unit control volume is given by

$$\bar{A}_{wa} = \frac{\text{area of wall in contact with phase "a"}}{\text{total fluid volume}} . \tag{3.6}$$

This quantity is calculated for all the total fluid volume flow regimes in Section 2. in the following.

3.1.1 Single Phase Flow Regimes

$$\bar{A}_{wa} = \frac{2\pi R\Delta x}{\pi R^2 \Delta x} = \frac{4}{D} \tag{3.7}$$

where

$$D = 2R .$$

3.1.2 Bubble, Froth, Dispersed, and Vertical Stagnation Regimes

The bubble, froth, dispersed, and vertical stagnation flow regimes are all assumed to be similar and the equations used to represent the area of each phase in contact with the wall are based on this area being proportional to the volume fraction of each phase. For a homogeneously and isotropically distributed mixture, the volume fraction of each phase is equal to the area fraction. Therefore, the wall area in contact with the gas phase is $\alpha 2\pi R\Delta x$ so that the wall area per unit volume is

$$\bar{A}_{wg} = \frac{\alpha 2\pi R\Delta x}{\pi R^2 \Delta x} = \frac{4\alpha}{D} . \tag{3.8}$$

Similarly, for the liquid,

$$\bar{A}_{w\ell} = \frac{(1-\alpha)\ 2\pi R\Delta x}{\pi R^2 \Delta x} = \frac{4(1-\alpha)}{D} . \tag{3.9}$$

The assumption that the dispersed phase is uniformly distributed in the continuous phase is a good approximation for adiabatic flow, but is in error when certain types of heat transfer from or to the stationary surface is considered. For example, changes in $A_{w\ell}$ should be made for the following conditions:

(1) Surface nucleate boiling. In this case most of the vapor bubbles are adjacent to the wall and not distributed throughout the continuous liquid phase. Thus Equation (3.8) understimates $\bar{A}_{wg}$ and Equation (3.9) overestimates $\bar{A}_{w\ell}$.

(2) Stable film boiling. For stable film boiling when the liquid is dispersed droplets ($\alpha>0.2$ assumed here), the dispersed drops do not touch the wall, so that $\bar{A}_{wg}$ should be the same as for single phase vapor. In this case, Equation (3.8) underestimates $\bar{A}_{wg}$ and Equation (3.9) overestimates $\bar{A}_{w\ell}$.

3.1.3 Annular, Slug, and Countercurrent (Liquid on Wall) Flow Regimes. All these regimes are treated as annular flow with liquid in contact with the wall. The liquid area per unit volume is

$$\bar{A}_{w\ell} = \frac{2\pi R\Delta x}{\pi R^2 \Delta x} = \frac{4}{D} \tag{3.10}$$

and for the gas phase,

$$\bar{A}_{wg} = 0 .$$

3.1.4 Inverse Annular and Countercurrent (Vapor on Wall) Flow Regimes. Both of these flow regimes are treated as inverse annular flow with vapor on the wall. The vapor area per unit volume is

$$\bar{A}_{wg} = \frac{2\pi R\Delta x}{\pi R^2 \Delta x} = \frac{4}{D} \tag{3.11a}$$

and for the liquid phase

$$\bar{A}_{w\ell} = 0 \tag{3.11b}$$

3.1.5 Separated and Horizontal Stagnation Regimes

The separated flow regime and the horizontal stagnation regime are assumed to be similar. The wall area per unit volume is related to the angle θ defined in Figure (3.2). This angle is related to the volume fraction of the gas phase by,

$$1 - \alpha = \frac{\text{volume of the liquid phase}}{\pi R^2 \Delta x}$$

$$1 - \alpha = \frac{\left[\frac{\theta}{2\pi}\ \pi R^2 - 2\left\{\frac{1}{2} R \sin\frac{\theta}{2} \quad R\cos\frac{\theta}{2}\right\}\right]\Delta x}{\pi R^2 \Delta x}$$

$$2\pi(1-\alpha) = \theta - \sin\theta \tag{3.12}$$

where θ is in radians.

Since Equation (3.12) is a transcendental fuction, θ cannot be written explicitly in terms of α but it can be solved for numerically.

The wall area of the gas phase per unit volume is

$$\bar{A}_{wg} = \frac{\frac{2\pi-\theta}{2\pi}\ 2\pi R\Delta x}{\pi R^2 \Delta x} = \frac{2(2\pi-\theta)}{\pi D} \tag{3.13a}$$

and for the liquid phase

$$\bar{A}_{w\ell} = \frac{2\theta}{\pi D} . \tag{3.13b}$$

3.2 Interphase Surface Area Per Unit Control Volume

The interphase surface area per unit control volume is computed from

$$\bar{A}_{g\ell} = \frac{\text{surface area between gas and liquid}}{\pi R^2 \Delta x} . \tag{3.14}$$

3.2.1 Single Phase. Since only one phase is present

$$\bar{A}_{g\ell} = 0 . \tag{3.15}$$

3.2.2 Bubble, Froth, Dispersed, and Vertical Stagnation Regimes. The interphase surface area for these flow regimes is dependent on the number of particles in the control volume, and the size of these particles. The particles in the dispersed phase are assumed to be spherical. The calculation of the average particle radius, r_p, is described in Section 3.5.

a) Bubbly flow: the number of bubbles in bubbly flow in a control volume of volume fraction α is

$$N = \frac{\alpha \pi R^2 \Delta x}{\frac{4}{3}\pi r_p^3} = \frac{3\alpha}{4} \frac{R^2 \Delta x}{r_p^3} . \tag{3.16}$$

The interfacial area per unit volume for these particles is given by

$$\bar{A}_{g\ell} = \frac{N 4\pi r_p^2}{\pi R^2 \Delta x} = 3 \frac{\alpha}{r_p} \tag{3.17}$$

The total number of bubbles is limited by the maximum packing which in turn limits the area. No limit for this effect is included other than the flow regime maps which are assumed to exclude selection of the bubbly flow regime for large values of α. Similar comments apply for dispersed flow for low values of α.

b) Dispersed flow: the interphase area for dispersed flow may be obtained from Equation (3.17) by replacing α by $1 - \alpha$ to obtain

$$\bar{A}_{g\ell} = 3 \frac{(1-\alpha)}{r_p} \tag{3.18}$$

c) Froth and Vertical Stagnation Regimes: for these regimes, $A_{g\ell}$ is assumed to agree with the bubbly regime when $\alpha \leq 0.5$ and with the dispersed regime when $\alpha > 0.5$.

$$\bar{A}_{g\ell} = \begin{cases} \dfrac{3\alpha}{r_p} & \alpha < 0.5 \\ \dfrac{3(1-\alpha)}{r_p} & \alpha > 0.5 \end{cases} \tag{3.19}$$

3.2.3 Annular, Slug, and Countercurrent (Liquid on Wall) Flow Regimes. The interphase surface area for annular flow is dependent on the film thickness. Figure (3.1) shows that the interphase surface area is given by the area of the inner cylinder of radius R_i and length Δx; that is,

$$\bar{A}_{g\ell} = \frac{2\pi R_i \Delta x}{\pi R^2 \Delta x} = \frac{2R_i}{R^2} \quad . \tag{3.20}$$

For a liquid film, the radius of the vapor volume center core fraction is related to α by

$$\alpha = \frac{\pi R_i^2 \Delta x}{\pi R^2 \Delta x} = \frac{R_i^2}{R^2} \tag{3.21}$$

so that $R_i = \sqrt{\alpha}\ R$. The area per unit volume is

$$\bar{A}_{g\ell} = \frac{2\pi\sqrt{\alpha}\, R\cdot\Delta x}{\pi R^2\cdot\Delta x} = \frac{4\sqrt{a}}{D} \quad . \tag{3.22}$$

3.2.4 Inverse Annular and Countercurrent (Vapor on Wall) Flow Regimes. For a vapor film, the radius of the liquid volume center core fraction is related to the volume fraction of gas as

$$\alpha = \frac{\pi(R^2-R_i^2)\Delta x}{\pi R^2\Delta x} = 1 - \frac{R_i^2}{R^2} \tag{3.23}$$

so that $R_i = \sqrt{1-\alpha}\, R$. The area per unit volume is

$$\bar{A}_{g\ell} = \frac{2\pi\sqrt{1-\alpha}\, R\ \Delta x}{\pi R^2\Delta x} = \frac{4\sqrt{1-\alpha}}{D} \quad . \tag{3.24}$$

3.2.5 Separated and Horizontal Stagnation Regimes. From Figure (3.2) the interphase surface area for separated flow is seen to be dependent on the angle θ determined in Equation (3.12) and the pipe radius,

$$\bar{A}_{g\ell} = \frac{2R\Delta x \mathrm{Sin}\ (\theta/2)}{\pi R^2\Delta x} = \frac{4\ \mathrm{Sin}\ (\theta/2)}{\pi D} \tag{3.25}$$

3.3 Stationary Surface Friction Coefficients and Wall Hydraulic Diameters

Correlations for surface friction coefficients should depend on the system parameters and not the independent variables such as space and time. The friction factors presented here comply with this requirement since steady state incompressible friction correlation are assumed to apply without modification to the transient compressible situation. The coefficient D_{wa} is related to the correct expression

for pipe flow. It is written in terms of the hydraulic diameter and the resulting expression is then assumed to apply to other geometries as long as the hydraulic diameter is used. The expression for the pressure drop, $\frac{dP}{dx}$, in a straight, constant area, circular pipe may be written in the form

$$\frac{dP}{dx} = -f \rho \frac{|v|v}{2D} .$$

where

f = friction factor corresponding to a laminer value of $64/Re$[a]

ρ = fluid density

v = velocity

D = diameter

Re = Reynolds number.

The momentum equation for a single phase incompressible, steady state fluid from Solbrig and Hughes, (1975), consistent with Equation (3.1) may be written as

$$\frac{dP}{dx} = -\bar{A}_{wa} B_{wa} v^a .$$

The area per unit volume is

$$\bar{A}_{wa} = \frac{2\pi R \Delta x}{\pi R^2 \Delta x} = \frac{4}{D} .$$

A combination of these three equations yields

$$B_{wa} = \frac{f\rho|v|}{8} .$$

---

[a] The Fanning friction factor f_f is defined as $f_f = \frac{1}{4}f$. It is used with an equation for pressure drop which is correspondingly modified as

$$\frac{dP}{dx} = 2f_f \rho \frac{|v|v}{D}$$

Although $\bar{A}_{wa}$ and B_{wa} are specified independently, the quantity of importance is the product of these two expressions.

The form for B_{wa} is extended to other geometries and flow regimes by

$$B_{wa} = \frac{f_a \rho_a |v^a|}{8} \tag{3.26}$$

where f_a is an appropriately defined friction factor and ρ_a is the thermodynamic density of phase "a". The friction factor, f, is a function of the Reynolds number and wall roughness for flow in a pipe (Knudsen and Katz, 1958). The well known Moody diagram is used as a basis for the friction factor for all flow regimes with an appropriate definition of the friction factor. The basic Moody diagram is modified for use here as described in the following.

In laminar flow in a round tube the friction factor is independent of wall roughness and is given by

$$f_a = \frac{64}{Re_w^a} \tag{3.27}$$

where Re_w^a is the Reynolds numbers of phase "a". The Reynolds number is given by

$$Re_w^a = \frac{D_w^a v^a \rho_a}{\mu_a} \tag{3.28}$$

where μ_a is the viscosity of phase "a" and D_w^a is the hydraulic diameter of phase "a" in contact with the wall. Thus for laminar flow,

$$B_{wa} = \frac{8\mu_a}{D_w^a} \tag{3.29}$$

The coefficient, B_{wa}, is calculated rather than f_a to eliminate the problem of the singularity in f_a encountered at $v^a = 0$.

In turbulent flow, the friction factor is determined from the Colebrook formula (Colebrook, 1938),

$$\frac{1}{\sqrt{f_a}} = -0.86 \ln \left[\frac{\varepsilon}{3.7 D_w^a} + \frac{2.51}{Re_w^a \sqrt{f_a}} \right] \tag{3.30}$$

where ε is the pipe roughness in terms of an average length of roughness protrusion and ln is the natural logarithm.

To ensure that a unique solution is achieved, we require that the friction factor be monotonic and continuous for given pipe roughness. A model which meets these requirements is sketched in Figure (3.3). If $Re_w^a > 4000$, turbulent flow is assumed to exist. In the transition region between laminar and turbulent flows, a horizontal straight line is drawn, connecting the turbulent friction factor at a Reynolds number of 4000 with the laminar friction factor curve. The intersection of this horizontal line with the laminar friction factor is a function of pipe roughness and lies in the approximate range $800 < Re_w^a < 1600$.

Experimental evidence (Knudsen and Katz, 1958, Chapter 7) supports extending Equation (3.30) to other geometries by using the hydraulic diameter defined as

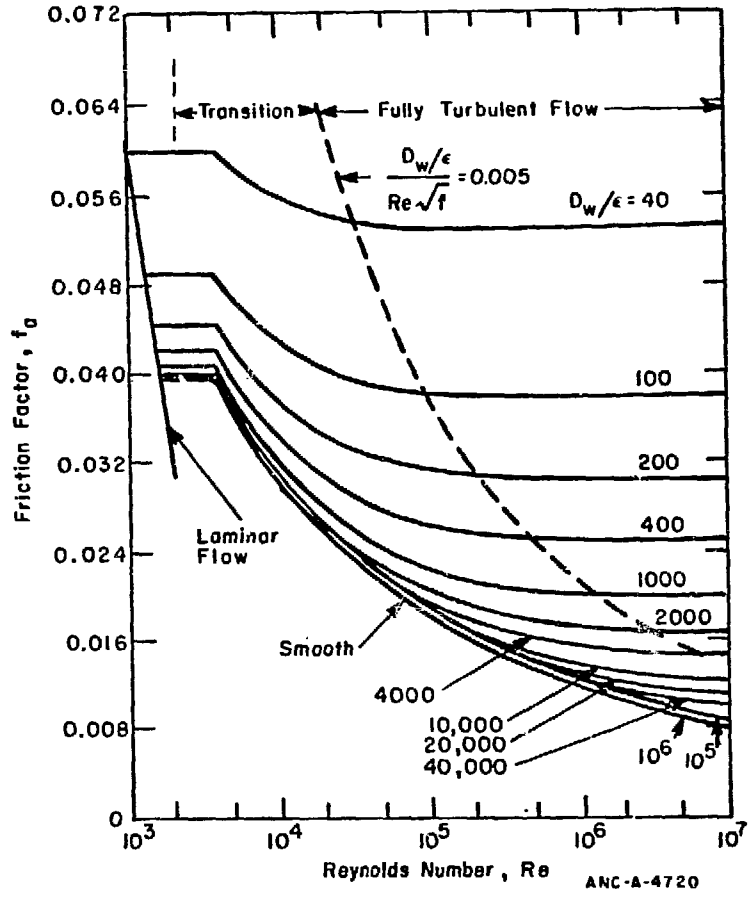

Figure 3.3 UVUT Friction Factor Model (Based upon Moody Diagram)

$$D_w = \frac{4 \text{ flow area}}{\text{wetted perimeter}}. \tag{3.31}$$

The use of Equation (3.27) for other geometries is known to be incorrect because it is geometry dependent. The form remains constant but the coefficient changes. The error incurred in using this equation for all geometries is assumed small. These equations are further extended to UVUT flow by defining the hydraulic diameter of phase "a" in contact with the wall as:

$$D_w^a = \frac{4 \text{ flow area of phase "a"}}{\text{wetted perimeter of phase "a" in contact with the wall}} \tag{3.32}$$

The reasonableness of this approach can be seen in Figure (3.4) for annular flow. A fit of experimental data of wall friction factors is compared to the laminar friction factor and the Blasuis equation (Knudsen and Katz, 1958, Chapter 7). The Blasius equation is a good fit to Equation (3.30) for large Reynolds number and smooth pipes. The definition of the wall friction factor is consistent with the definition used in the UVUT theories and represents only the force on the wall.

The assumption that friction factors can be used to represent the shear stress at the wall even during a transient has been investigated by Slattery (1972, p 182) for a simple problem. The basic assumption involved is that the shear at the wall can be related to the average velocity in the pipe. An approximation is involved here because many different velocity profiles can have the same average velocity. If the flow situations are restricted to cases for which the profiles are similar, this assumption is reasonable. In order to investigate the approximation involved in using steady state friction factors, Slattery obtained

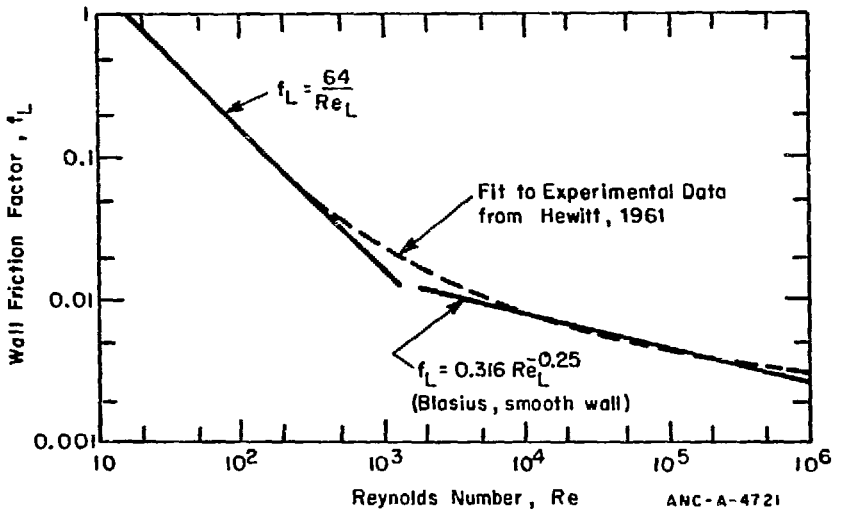

Figure 3.4 Comparison of Friction Factor Empirical Fit to Data of Hewitt (1961) with Standard Values for Full Pipe Flow

a solution with a pressure gradient imposed on an incompressible fluid initially at rest. He solved the problem two ways. The first involved the exact solution of the equation

$$\rho\frac{\partial v}{\partial t} = -\frac{\partial p}{\partial x} + \mu\frac{1}{r}\frac{\partial}{\partial r}\left(r\frac{\partial v}{\partial r}\right) \tag{3.33}$$

where v is the velocity in the axial direction x and r is the radial direction. The second involved the solution of the equation

$$\rho\frac{\partial \bar{v}}{\partial t} = -\frac{\partial p}{\partial x} - f\frac{\rho|\bar{v}|\bar{v}}{2D} \tag{3.34}$$

where

$$\bar{v} = \frac{1}{\pi R^2}\int_0^{2\pi}\int_0^{R} v r dr d\theta$$

$$f = \frac{64}{Re}$$

R = radius of the pipe .

The solutions are presented in Figure (3.5) in terms of the average velocity as a function of time.

The conclusion reached by Slattery is that the friction factor approach underestimates transient instantaneous wall shear for all times for accelerating flow and hence the velocity is higher than that computed from the exact solution. Slattery concluded that the 20 to 25 percent disagreement (average) for $\frac{\mu t}{\rho R^2} > 0.04$ is satisfactory for many enineering applications. If this trend holds in general for laminar and turbulent multiphase transient flows, then velocities calculated from UVUT theories would be higher than actually encountered for accelerating flows. Lower velocities may result for decelerating flow.

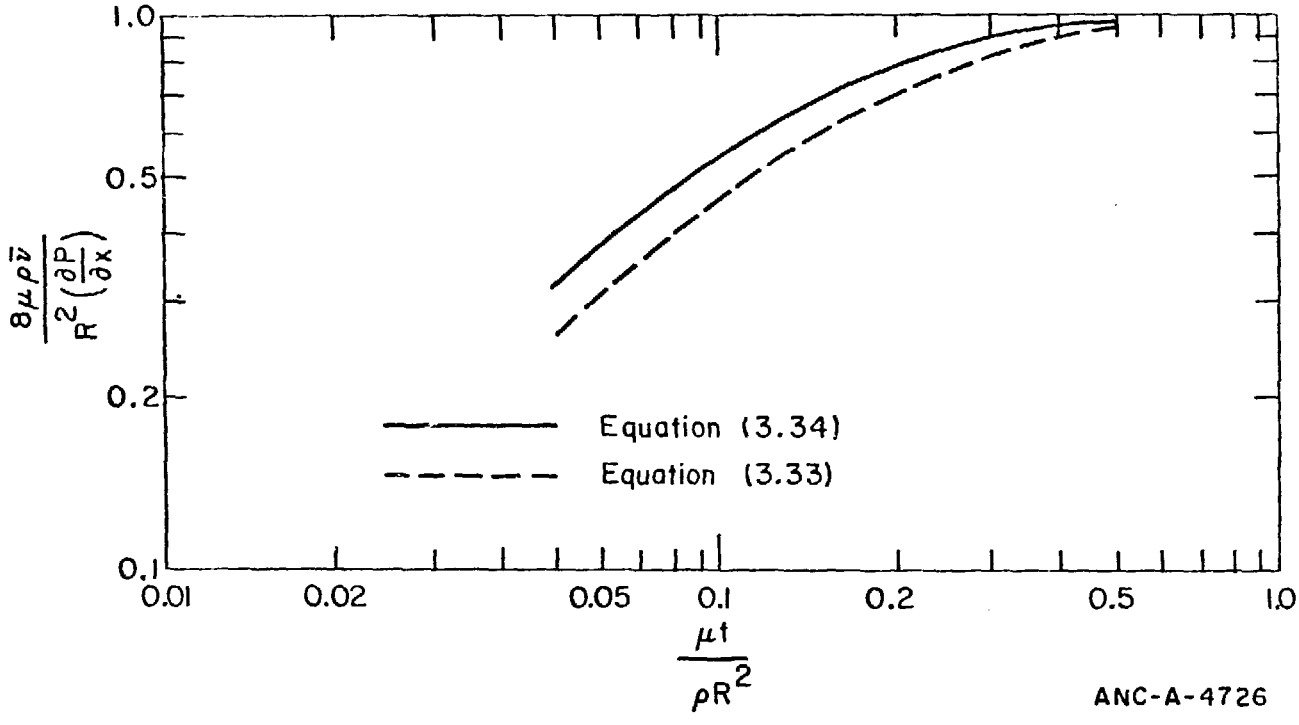

Figure 3.5 Comparison of Area-Averaged Analysis with exact Solution for Flow from Rest in a Circular Tube (Slattery, 1972)

In order to use the UVUT friction factor model, the appropriate hydraulic diameter must be used. The present models for the various flow regimes are presented in the following and are based on Equation (3.32).

3.3.1 Single Phase Flow Regimes. The hydraulic diameter is, of course, just the pipe diameter

$$D_w^a = \frac{4\ \pi R^2}{2\pi R} = D \quad . \tag{3.35}$$

3.3.2 Bubble, Froth, Dispersed, and Vertical Stagnation Regimes. The geometry for each phase explained in Section 3.1.2 implies that for the gas phase,

$$D_w^g = \frac{4\ \alpha\pi R^2}{2\alpha\pi R} = D \tag{3.36}$$

and for the liquid phase

$$D_w^\ell = \frac{4\ (1-\alpha)\pi R^2}{2(1-\alpha)\pi R} = D \quad . \tag{3.37}$$

3.3.3 Annular, Slug, and Countercurrent (Liquid on Wall) Flow Regimes. The wall hydraulic diameter for the liquid is

$$D_w^\ell = \frac{4\ (1-\alpha)\pi R^2}{2\pi R} = (1-\alpha)\ D \quad . \tag{3.38}$$

Since the gas phase is not in contact with the wall, D_w^g is not needed.

3.3.4 Inverse Annular and Countercurrent (Vapor on Wall) Flow Regimes. Vapor is in contact with the wall in this flow regime so that

$$D_w^g = \frac{4\ \alpha\pi R^2}{2\pi R} = \alpha D \quad . \tag{3.39}$$

The liquid phase is not in contact with the wall, so D_w^ℓ is not needed.

3.3.5 Separated and Horizontal Stagnation Regimes. The geometry of this regime has been derived in Section 3.1.5 where θ was related to α in Equation (3.12). The wall hydraulic diameter for the gas phase is

$$D_w^g = \frac{4\ \alpha\pi R^2}{\frac{2\pi-\theta}{2\pi}\ 2\pi R}$$

$$= \frac{2\pi\alpha D}{2\pi-\theta} \qquad (3.40)$$

and for the liquid phase

$$D_w^\ell = \frac{4\ (1-\alpha)\ \pi R^2}{\frac{\theta}{2\pi}\ \ 2\pi R}$$

$$= \frac{2\pi(1-\alpha)\ D}{\theta}\ . \qquad (3.41)$$

The ratio of the hydraulic diameter of the gas phase to the tube diameter is plotted in Figure (3.6) for illustrative purposes.

3.4 Interphase Friction Coefficients and Interphase Hydraulic Diameter

A consistent definition of the interphase coefficients is

$$B_{ab} = \frac{f_a\ \rho_a\ |\ v^a - v^*}{8} \qquad (3.42)$$

where v^* is the velocity at the interface between the two phases.

The interface velocity may be solved for by requiring that the sum of the interface friction forces is zero

$$B_{g\ell}\ (v^g - v^*)\ +\ B_{\ell g}\ (v^\ell - v^*) = 0\ .$$

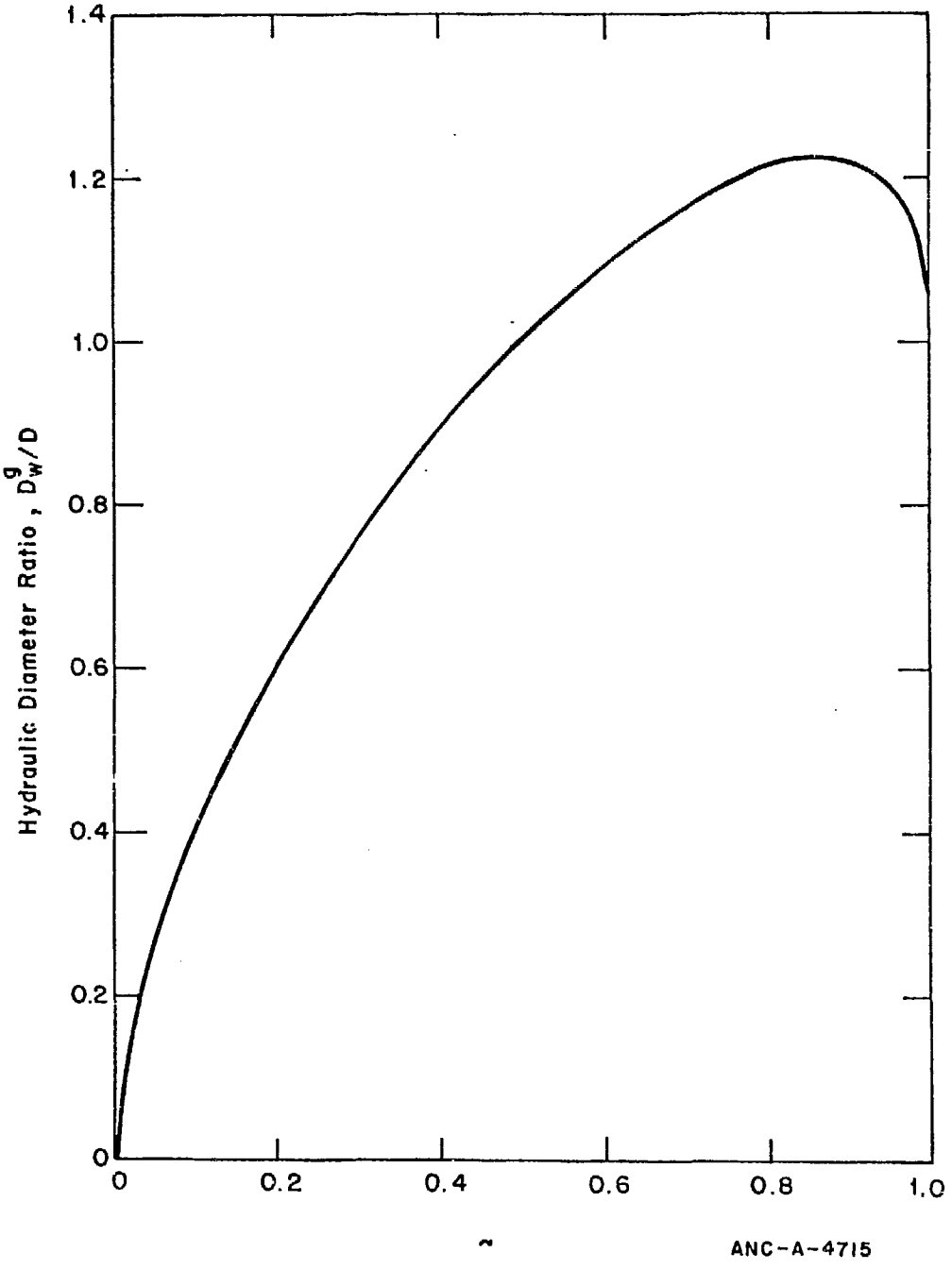

Figure 3.6 Hydraulic Diameter for Separated Flow

The assumption is made that $v^g > v^* > v^\ell$ and Equation (3.42) is substituted into Equation ( ), then

$$F(v^*) = 0$$

is solved, where

$$F \equiv f_g\rho_g\,(v^g - v^*)^2 - f_\ell\rho_\ell\,(v^\ell - v^*)^2$$

or

$$F = (f_g\rho_g - f_\ell\rho_\ell)v^{*2} - 2(f_g\rho_g v^g - f_\ell\rho_\ell v^\ell)v^* + (f_g\rho_g\, v^{g^2} - f_\ell\rho_\ell v^{\ell^2}) \ .$$

If the products $f_i\rho_i$ are assumed independent of velocity, then the solution for v^* is

$$v^* = \frac{(f_g\rho_g v^g - f_\ell\rho_\ell v^\ell) \pm \sqrt{f_g\rho_g f_\ell\rho_\ell}\ (v^g - v^\ell)}{(f_g\rho_g - f_\ell\rho_\ell)} \ .$$

Only one of these roots is physically real as seen in the following. Since F is a quadratic function in v^*, it can have only one maximum or minimum. The derivative is

$$\frac{dF}{dv^*} = 2\,(f_g\rho_g - f_\ell\rho_\ell)v^* - 2(f_g\rho_g v^g - f_\ell\rho_\ell v^\ell) \ .$$

if the derivative is evaluated at v^g and v, then

$$\frac{dF}{dv^*}\,(v^g) = -2f_\ell\rho_\ell\,(v^g - v^\ell) \quad < 0$$

$$\frac{dF}{dv^*}\,(v^\ell) = -2f_g\rho_g\,(v^g - v^\ell) \quad < 0 \ .$$

Since the derivative has the same sign at these two points, no maximum or minimum can occur between these two points. A solution does occur between these two points because

$$F(v^g) = -f_\ell\rho_\ell\,(v^\ell - v^g)^2 \quad < 0$$

$$F(v^\ell) = f_g\rho_g(v^g - v^\ell)^2 > 0 \ .$$

The root desired is obtained by evaluating the root for any convenient set of conditions

such as $v^g = 2v^\ell$ and $f_g\rho_g = 2f_\ell\rho_\ell$

so that $v^* = (3\pm\sqrt{2})\ v^\ell$.

Therefore, the negative root is required in order to satisfy the original assumption that $v^g > v^* > v^\ell$ so that in general

$$v^* = \frac{(f_g\rho_g\ v^g - f_\ell\rho_\ell v^\ell) - \sqrt{f_g\rho_g f_\ell\rho_\ell}\ (v^g - v^\ell)}{(f_g\rho_g - f_\ell\rho_\ell)} \quad . \tag{3.43}$$

In the degenerate case when $f_g\rho_g = f_\ell\rho_\ell$, L' Hospital's rule can be used to evaluate Equation (3.43) as

$$v^* = \frac{1}{2}\ (v^g + v^\ell) \quad .$$

Equation (3.43) is a general solution and is also obtained when $v^g < v^* < v^\ell$.

Similar expressions could be obtained for laminar flow or combinations of laminar and turbulent flow. When $f_g \simeq f_\ell$, $v^g \simeq v^\ell$, and $\rho_g << \rho_\ell$, then $v^* \simeq v^\ell$.

The interphase Reynolds number is based on the interface velocity as a reference velocity and is defined for each phase as

$$Re^a_{int} = \frac{|v^a - v^*|\ D^a_{int}\ \rho_a}{\mu_a} \tag{3.44}$$

The friction factor for each flow regime is identified in the following. The general observation is made that the modified Moody diagram (Figure 3.3) is used in annular and separated type flow regimes and that friction factors or drag coefficients obtained for flow over spheres is used for dispersed type flow regimes.

3.4.1 Single Phase Flow. No interphase friction occurs for single phase flow so

$$B_{ab} = 0 \quad . \tag{3.45}$$

3.4.2 Bubble, Froth, Dispersed, and Vertical Stagnation Regimes. In all these flow regimes, the friction models used are based on the assumption that the continuous fluid is flowing over a rigid sphere. The equation used in the literature for the force on a submerged object is

$$F = C_D A_p \rho_c \frac{U^2}{2} \tag{3.46}$$

where F = the force on the submerged object

C_D = the drag coefficient

A_p = the projected area of the object on a plane normal to the flow direction

ρ_c = the density of the continuous phase.

U = the velocity of the fluid relative to the object.

The commonly used drag coefficient must be related to the friction factor used in this study. Equation (3.46) can be written as

$$F_{CD} = \frac{A_{CD}}{V_C} \frac{A_p}{A} 4C_D \frac{\rho_c \left| v^C - v^D \right|}{8} (v^C - v^D) \tag{3.47}$$

to express the force per unit volume in a control volume with many submerged objects of the same size and shape, where

F_{CD} = the force per unit volume between the continuous and dispersed phases in the control volume V_C.

A_{CD} = the total area between the continuous and dispersed phases in the control volume V_C

A = the surface area of a single particle

v^C = the velocity of the continuous phase

and v^D = the velocity of the dispersed phase.

In this equation the velocity of the dispersed phase is assumed to be the interface velocity.

In general, the friction factor can be identified with

$$f_c = \frac{A_p}{A} 4C_D . \tag{3.48a}$$

In particular, for the case of spheres ($A_p = \pi r^2$ and $A = 4\pi r^2$)

$$f_c = C_D . \tag{3.48b}$$

The force F_{DC} is evaluated as $F_{DC} = - F_{CD}$. The form for C_D is taken from a fit of experimental data for flow over spheres (Clift and Gauvin, 1971)

$$f_{CD} = \frac{24}{Re_p} \left[1 + 0.15\ Re_p^{0.687}\right] + \frac{0.42}{1 + 4.25 \times 10^4\ Re_p^{-1.16}} . \tag{3.49}$$

The use of the friction coefficient $B_{g\ell}$ eliminates the singularity difficulty in using f_i when the velocities are equal. The particle Reynolds number is defined as

$$Re_p = \frac{\left| v^C - v^D \right| 2r_p \rho_c}{\mu_c} \tag{3.50}$$

where the interphase hydraulic diameter is $D^c_{int} = 2r_p$.

The range over which Equation (3.50) is valid has been investigated by Clift and Gauvin (1971) and found to be $Re_p < 10^5$. This function is plotted in Figure (3.7) and appears to be reasonable to use for all Reynolds numbers. For low Reynolds numbers, the function approaches the theoretical stokes solution and at large Reynolds number it approaches a constant value of 0.42. The friction factors are noted to be much higher than pipe friction factors for the same Reynolds number, except at low Reynolds numbers. In fact, the fully developed friction factor would correspond to a relative roughness of $D_w/\varepsilon = 1.59$ on Figure (3.3).

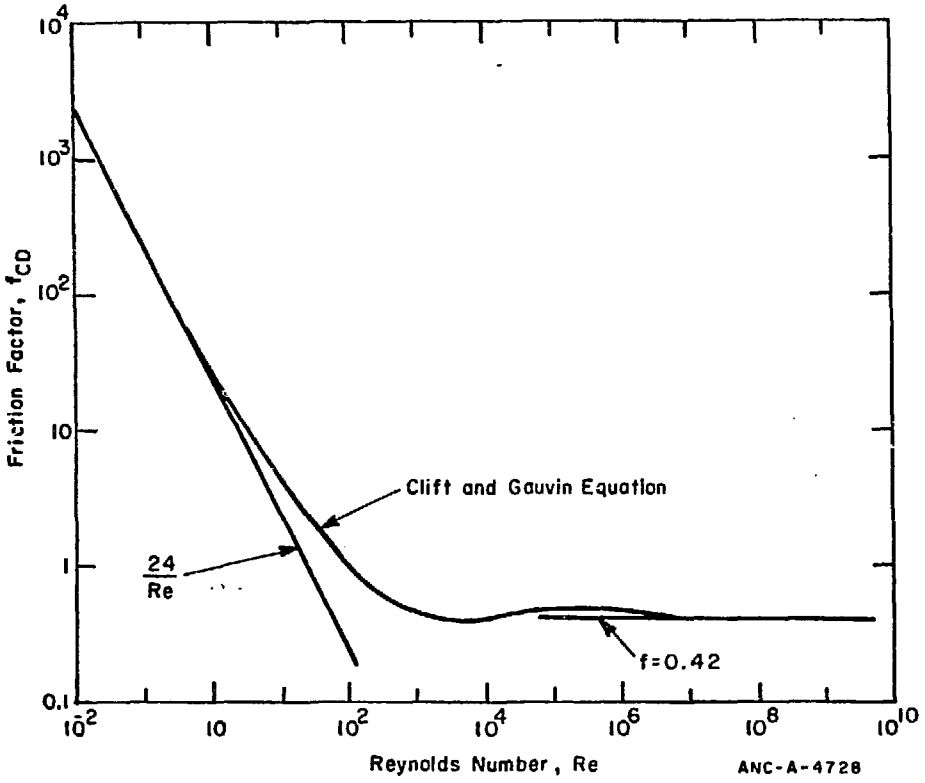

Figure 3.7 Friction Factors for Spheres

3.4.3 Annular, Slug, Countercurrent (Liquid on Wall) Flow Regimes. All of these regimes are treated as an annular flow geometry. The interphase friction can be written for the gas center core for steady state as (Wallis, 1969)

$$-\frac{\partial P}{\partial x} = \frac{2C_{fi}\rho_g \left| v^g - v^* \right| (v^g - v^*)}{D^g_{int}} \tag{3.51}$$

where C_{fi} is the Fanning friction factor. Since $D^g_{int} = D\sqrt{\alpha}$, this equation can be written as

$$-\frac{\partial P}{\partial x} = \frac{f_i \rho_g \left| v_g - v^* \right| (v^g - v^*)}{2D\sqrt{\alpha}} \tag{3.52}$$

where $f_i = 4C_{fi}$.

The gas phase momentum equation neglecting all terms except the pressure drop and the interphase friction is

$$F_{g\ell} = -\alpha\frac{\partial P}{\partial x} = \bar{A}_{g\ell} B_{g\ell} (v^g - v^*) \tag{3.53}$$

where $F_{g\ell}$ is the interphase friction force.

Appropriate identification of the terms in this equation can be made by multiplying Equation (3.52) by α and substituting $\bar{A}_{g\ell} = 4\sqrt{\alpha}/D$ into Equation (3.53) and equating the two expressions

$$\frac{\alpha f_g \rho_g \left| v^g - v^* \right| (v^g - v^*)}{2D\sqrt{\alpha}} = \frac{4\sqrt{\alpha}}{D} B_{g\ell} (v^g - v^*)$$

or

$$B_{g\ell} = \frac{f_g \rho_g \left| v^g - v^* \right|}{8} \tag{3.54}$$

which is consistent with the usual definition of $B_{g\ell}$.

The viscosity of water is much higher than that of the vapor so that a good approximation for annular flow is to use the gas phase to evaluate the interphase friction with v^* approximated by the velocity of the liquid. Substitution of $v^* = v^\ell$ into the gas phase expression (Equation 3.53) for the interphase force, along with Equation (3.54) yields

$$\underset{\sim}{F}_{g\ell} = -F_{\ell g} = \frac{4\sqrt{\alpha}}{D} \frac{f_g \rho_g |v^g - v^\ell|}{8} (v^g - v^\ell) . \tag{3.55}$$

The Reynolds number is

$$Re^g_{int} = \frac{|v^g - v^\ell| D\sqrt{\alpha}\, \rho_g}{\mu_g} \tag{3.56}$$

The friction factor is evaluated from the work of Moeck (1970 pp 164 to 169) and Wallis (1969 pp 318 to 323). (Wallis and Moeck use the Fanning friction factor definition which is a factor of four less than the one used here. In reporting their work in this paper, the Fanning friction factors have been converted to the ones used here). Experimental data which these references obtained from literature covers a range of film thicknesses, δ, from $\delta/R = 0$ to $\delta/R = 0.1$. This film thickness range corresponds to a range of α from $1 \leq \alpha \leq 0.81$. The data reported by Moeck correspond to large Reynolds numbers. If these data were plotted on Figure (3.3), all of the data would fall in or near to the region where the friction factor depends only on roughness and is independent of Reynolds number. Since the friction factors are above those representing the curve for smooth pipes, the waves and ripples on the surface of the liquid are interpreted as roughness relative to the flow of the vapor. Consequently, to relate the experimental data to the roughness is desirable and has been done by Wallis (1969). He represented the data by the equation

$$f_g = 0.02 \left(1 + 300 \frac{\delta}{D_w}\right) \tag{3.57}$$

Equation (3.57) also represents the data presented by Moeck (1970) adequately although Moeck presents a different relation which is

$$f_g = 0.02 \left[1+545 \left(\frac{\delta}{R} \right)^{1.42} \right] . \tag{3.58}$$

Wallis also pointed out that the equation which represents the friction factor in the Reynolds number independent regime (Knudsen and Katz, 1958)

$$\frac{2}{\sqrt{f}} = 4 \log \frac{r_w}{\epsilon} + 3.48 \tag{3.59}$$

can be represented by the equation

$$f = 0.02 \left(1 + 75 \left(\frac{\epsilon}{D_w} \right) \right) . \tag{3.60}$$

Wallis concluded by comparing Equations (3.57) and (3.60) that the roughness of the interface could be represented by

$$\frac{\epsilon}{D_w} = 4 \frac{\delta}{D_w}$$

Figure (3.8) presents Equations (3.57) to (3.60). Equation (3.59) does differ from Equation (3.60) with the consequence that for equal friction factors, ϵ can differ from δ by as much as a factor of eight; however, four is a reasonable approximation and will be used here. Since the experimental data only apply to the range of $1 \geq \alpha \geq 0.81$, the correlation must be extended to other void fractions. Clearly Equation (3.61) cannot hold for $\frac{\delta}{D} > 0.2$ since 0.2 is the value which would cause the waves to span the pipe. The film thickness is related to the volume fraction of gas by

$$\frac{\delta}{R} = 1 - \sqrt{\alpha} \tag{3.62}$$

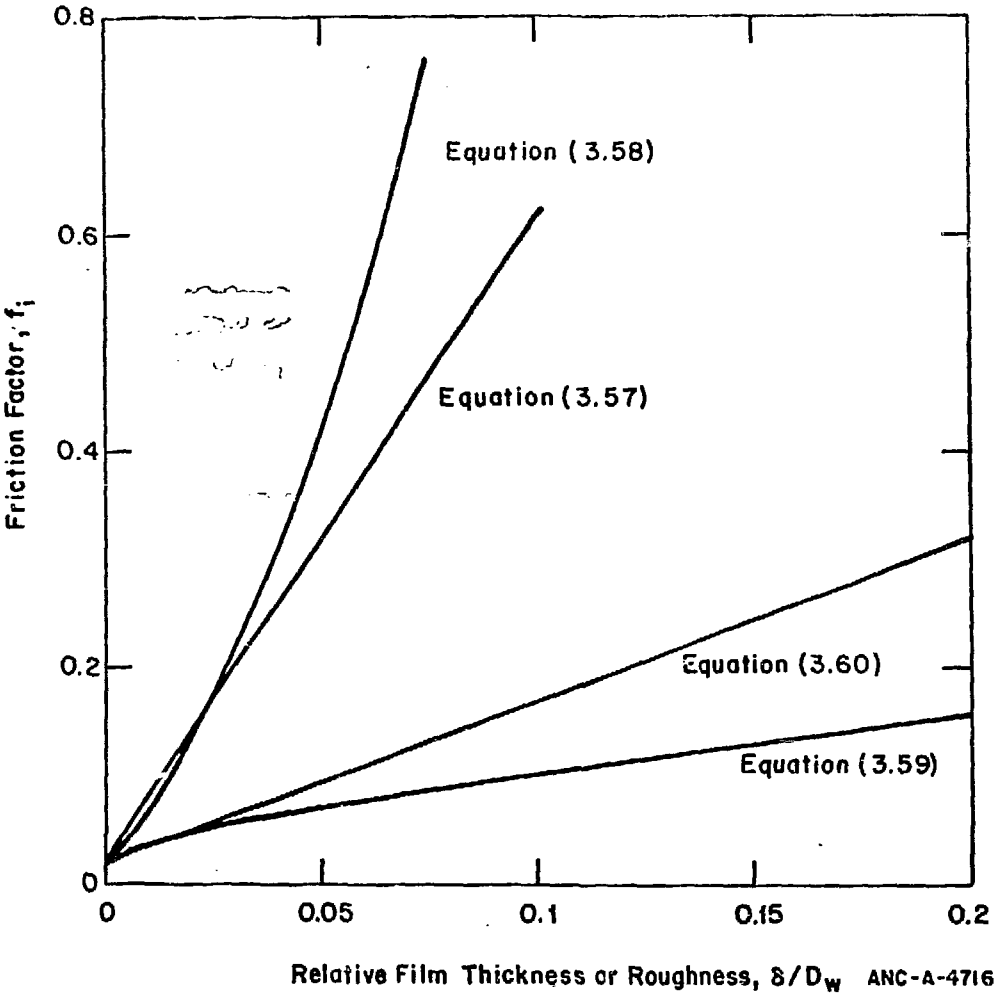

Figure 3.8 Determination of Equivalent Roughness

The model adopted for determining the roughness is

$$\left.\begin{aligned} \frac{\varepsilon}{D_w} &= 4\,\frac{\delta}{D_w} && 0 \le \frac{\delta}{D_w} \le 0.05 \\ \frac{\varepsilon}{D_w} &= 0.4 && 0.05 \le \frac{\delta}{D_w} \le 1.0 \end{aligned}\right\} \qquad (3.62)$$

The value, $\delta/D = 0.05$ was used as a cut off point because data do not exist above that and the roughness is very high at this value. Annular flow would probably not be selected by a flow regime map when δ/D is large; however, the above model does yield reasonable values in any case. The fact that large waves will break off as droplets and that this effect is not treated by the current model is recognized.

After the relative roughness has been determined, the modified Moody diagram [(Equations (3.27) and (3.30)] is used to determine the friction factor. Equation (3.56) is used to evaluate the Reynolds number. A correction should be made for the effect of velocity difference on the wave height. However, since the wave height would decrease with decreasing velocity difference and the laminar flow friction factor, which is independent of roughness, is used for small velocity differences, the neglect of the effect of velocity difference is probably insignificant.

3.4.4 Inverse Annular and Countercurrent (Vapor on Wall) Flow Regimes. The same model as used for annular flow is used to determine the wave height with the exception that the water depth is determined from the center core radius as

$$\frac{\delta}{R} = 1 - \sqrt{1-\alpha} \qquad (3.63)$$

The relative roughness or wave height is determined from Equation (3.62). Also, for this flow regime v^* is assumed to be approximated by v^{ℓ} and the interphase friction force is assumed to be evaluated using gas phase properties. Equations (3.51) through (3.56) are used with α replaced by $1 - \alpha$. The Moody diagram is used to determine the friction factor from the Reynolds number and the relative roughness.

3.4.5 Separated and Horizontal Stagnation Regimes. The same wave height model as used for annular flow is used for the separated and horizontal stagnation except that the water depth is approximated from the depth at the center line. As observed from Figure (3.2) the water depth is

$$\frac{\delta}{R} = (1 - \cos \frac{\theta}{2}) \tag{3.64}$$

where, θ is related to α by Equation (3.12). Due to the approximations involved, the maximum depth is used rather than an average depth which would require that the model be refined. The relative roughness (or wave height) is determined from Equation (3.62). The gas interphase hydraulic diameter calculated from the usual definition is

$$D^g_{int} = \frac{4\alpha\pi R^2}{2\ R \sin (\frac{\theta}{2})}$$

or

$$D^g_{int} = \frac{2\alpha\pi R}{\sin (\frac{\theta}{2})} \tag{3.65}$$

This expression approaches infinity as α approaches unity. Since the hydraulic diameter is used in the Reynolds number to obtain a measure of the turbulence, Equation (3.65) is considered unrealistic either because it considers too much fluid or too little perimeter. The assumption is made that the turbulence level of the gas phase would be similar to that for annular flow. The preceding definition

is modified to include the entire perimeter of the gas phase. This modification agrees with the definition used by Govier and Aziz (1972)

$$D^g_{int} = \frac{4\alpha\pi R^2}{2\,R\,\sin\left(\frac{\theta}{2}\right) + \frac{2\pi-\theta}{2\pi}\,2\pi R}$$

$$D^g_{int} = \frac{2\alpha\pi R}{\sin\left(\frac{\theta}{2}\right) + \pi - \frac{\theta}{2}} \tag{3.66}$$

Equation (3.44) is used as the Reynolds number definition. The interphase friction is evaluated by using the gas phase friction and approximating v^* by v^ℓ. The Moody diagram, Figure (3.3) is used to determine the friction factor.

3.5 Particle Radius

For all flow regimes for which a bubble or droplet diameter is required, in the model, the following model developed by Mugele and Evans (1951) as applied by Moeck (1970, p 136) for drcplets is used. A distribution was obtained by Mugele and Evans for the droplets in terms of the maximum droplet radius. A volume mean droplet radius, r_p, was obtained as

$$\frac{r_p}{r_{max}} = \left[1 + 3\,a\,\exp\left(1/4\delta^2\right) + 3\,a^2\,\exp\left(1/\delta^2\right) + a^3\,\exp\left(9/4\delta^2\right)\right]^{-\frac{1}{3}} \tag{3.67}$$

The recommended values of a and δ are (Moeck, 1970)

$$a = 4$$

$$\delta = 0.738$$

so that

$$\frac{r_p}{r_{max}} = 0.06147 \tag{3.68}$$

The maximum particle radius is calculated from the critical Weber number which is defined here as

$$We_{crit} = \frac{2\, r_{max}\, \rho_c\, (v^g - v^\ell)^2}{\sigma} \tag{3.69}$$

where

ρ_c = thermodynamic density of the continuous phase

and

σ = surface tension.

The values used for the critical Weber numbers are

$$We_{crit} = 13 \text{ drops} \tag{3.70}$$

$$We_{crit} = 1.24 \text{ bubbles}. \tag{3.71}$$

The value for droplets is taken from a best fit of data by Moeck (1970, p 134). The critical Weber number for bubbles is based on bubble breakup due to turbulent flow (Sevik and Park, 1973). It is recognized that this model does not accurately represent bubble size and growth rate during nucleate boiling, but considers only the effect of mechanical forces on the bubble. The use of Equation (3.69) to determine the particle size can produce large values when the velocities are nearly equal. The value of r_p is limited by the radius that would be obtained if the flow regime were annular. That is,

for drops, and

$$r_p \leq \sqrt{1-\alpha}\, R \tag{3.72}$$

$$r_p \leq \sqrt{\alpha}\, R \tag{3.73}$$

for bubbles.

4. INTRINSIC VELOCITIES

The phase change processes of evaporation of the liquid phase and condensation of the vapor phase can occur due to energy transfer from stationary surfaces within or bounding the flow field, energy transfer between the phases, and the existence of a pressure change. The effect of the mass exchange process on the momentum of a phase is represented by a term of the form $\dot{m}^a \hat{v}_i^a$ (Solbrig and Hughes, 1975) where $\dot{m}^a$ is the mass generation rate of phase "a" (from phase "b") and $\hat{v}_i^a$ is the intrinsic velocity of mass generation. These processes occur at the interface between the phases within the control volume. In general, the interface moves with its own intrinsic velocity $\hat{v}_i^a$ and not with the velocity of either phase.

For unequal phase temperature fluids experiencing a pressure change, condensation and evaporation can occur due to the several processes previously mentioned. Only one velocity is used to represent the velocity of mass generation of phase "a" at the current time although use of a different velocity for each of the several processes is conceptually possible. The intrinsic velocity $\hat{v}_i^a$ is an unknown for each phase. It should be related to the velocity $\hat{v}_i^a$ and other quantities. Some controversey exists in the literature as to whether these relations should both be constitutive equations or whether one should be replaced with a momentum balance. The latter view is accepted in this paper for the following reason.

When a particle of mass, m, leaves phase "a" and enters phase "b" it does not change its center of mass when changing phase. On a continuum basis, no time or force is required to change phase. Change of phase of a mass simply means that a different equation is used to account for the momentum of that mass. The momentum of the mass exchanged must be conserved in the phase transition. That is,

$$m \hat{v}_i^a = m \hat{v}_i^b$$

or (4.1)

$$\hat{v}_i^a = \hat{v}_i^b \equiv \hat{v}_i$$

which states that the intrinsic velocities are equal. This relation would conflict with the assumption of setting the intrinsic velocity of a phase equal to the velocity of the phase. That is, the relations

$$\hat{v}_i^a = v_i^a \tag{4.2}$$

cannot be valid except in the degenerate case for which the velocities of both phases are always equal. Thus, the Equation (4.2) is dismissed as being, in general, not applicable to an equal phase pressure seriated continuum.

An additional equation is necessary to relate $\hat{v}_i$ to other variables. This relation is a constitutive equation which can depend on the flow regime. This relation will be represented by the following

$$\hat{v}_i = \hat{v}_i\ (v_i^g,\ v_i^\ell) \tag{4.3}$$

where g refers to the gas phase

ℓ refers to the liquid phase

Other variables might be included in the argument list of Equation (4.3) for some flow regimes. Some possibilities for the function $\hat{v}_i$ are given in but not restricted to the following:

$$1)\quad \hat{v}_i = v_i^g \quad \text{when } \dot{m} < 0 \tag{4.4}$$

$$\hat{v}_i = v_i^\ell \quad \text{when } \dot{m} > 0$$

where $\dot{m}$ is the mass exchange rate of liquid into vapor.

This relation implies that the intrinsic velocity is equal to the velocity of the phase that is losing mass and is the model used here.

$$2) \quad \hat{v}_i = v_i^a \tag{4.5}$$

where "a" is the dispersed phase.

Equation (4.5) may be derived by considering the flow from or to a droplet uniform in all directions. The vapor leaves the surface with a velocity relative to the surface of

$$v_n = \frac{\dot{m}}{\rho_g A}$$

where v_n is the velocity normal to the surface. The average value of this velocity in any direction is zero. Therefore, the average vapor leaves the droplet at the velocity of the droplet.

$$3) \quad \hat{v}_i = \beta\, v_i^g + (1 - \beta)\, v_i^\ell \tag{4.6}$$

where β is a weighting factor ($0 \leq \beta \leq 1$). This relation implies that a continuous velocity distribution occurs between the gas and liquid phases. When β is between zero and unity, the interface velocity is bounded by these two velocities.

A brief literature review is included in the following to summarize what other authors have used. Panton (1968) who analyzes a gas-particle mixture assumes that the velocity of the dispersed phase, Equation (4.5), should always be used. Green and Naghdi (1969) and Craine, Green, and Naghdi (1970) analyze a multicomponent mixture and hypothesize that $\hat{v}_i^a$ is a mean velocity which will depend on the velocities of the remaining components. The simplest expression which satisfies this hypothesis for a two phase mixture is

$$\hat{v}_i^a = v_i^b \tag{4.7}$$

This expression conflicts with Equation (4.1) except when the velocities are equal. Naghdi, in a private communication,[a] indicated that $\hat{v}_i^a$ should also be included. This modification would be consistent with Equation (4.6). Müller (1968) indicates that the momentum growth consists of two parts: 1) thermal-mechanical interactions; and 2) phase change (chemical production). The latter portion is equivalent to the momentum growth considered in this section. He states that $\hat{v}_i^a$ is the velocity of the newly created mass. The first part is presumably related to diffusive forces which are considered nonexistent in a two phase mixture. Marble (1969) states that as a result of condensation or vaporization at the droplet surface, mass is transferred between the velocities of the bulk liquid and bulk vapor. Such mass transfer is consistent with Equation (4.6). The particular problem he considers is liquid droplets dispersed in a steam environment. He states that with the assumption of no shear induced circulatory motion, the mass exchanged at the interface has the velocity of the liquid phase. This mass exchange is consistent with Equation (4.5).

Mecredy and Hamilton (1972) subdivide the mass exchange process into an evaporation rate Γ_e and a condensation rate, Γ_c. These rates are related to the mass exchange in the present work by the relation

$$\dot{m} = \Gamma_e - \Gamma_c \tag{4.8}$$

Expressions from kinetic theory are used to compute Γ_e and Γ_c. The momentum growth of the gas phase is defined by Mecredy and Hamilton as

$$\Gamma_e v_i^{\ell} - \Gamma_c v_i^{g} \tag{4.9}$$

---

[a] Personal communication, P. M. Naghdi, University of California, Berkeley, to J. A. Trapp, Aerojet Nuclear Company (August 1974)

where ℓ and g refer to the liquid phase and gas phase, respectively. These expressions were not used in the present work because they predict that $\dot{m} = 0$ for equal phase temprature, which precludes a net evaporation or condensation during a pressure change and appears to be physically unrealistic for the present work.

The conclusion which might be drawn from the literature is that no agreement has been reached as to what this term should be; however, we believe that the conclusion which should be drawn is that no universal method exists for computing the intrinsic velocity, $\hat{v}_i$. The method of calculation will depend on the flow regime. Consequently, the intrinsic velocity calculation should be done with a correlation which is dependent on the two phase flow regime. As noted by Panton (1968) for the case in which averages are used to eliminate solving for three dimensional velocity distributions around single particles, an assumption, or model, regarding the distribution of the mass exchange process around a droplet or bubble is required. For example, if evaporation is occurring uniformly around a droplet no net effect results on the momentum of the droplet. If condensation is occurring on one half of the droplet and evaporation on the other half, an effect would result. However, with only averaged information available, directional effects associated with the mass exchange processes cannot be accounted for unless these effects are included through correlations for $\hat{v}_i$.

The model which is currently used in the SLOOP code is Equation (4.4). The $\dot{m}^a$ used is based on the net mass exchange between phases so that only a single intrinsic velocity, the velocity of the phase from which the mass is coming, is used in the momentum growth term. This model is used for all flow regimes. Other models which have been used have been discarded because they yielded physically unrealistic results. For example, when $\hat{v}_i$ was set equal to the velocity of the dispersed phase independent of $\dot{m}$ unrealistic results were produced.

5. HEAT TRANSFER REGIME MAPS

The UVUT theories require heat transfer coefficients and energy distribution functions which are heat transfer regime and flow regime dependent. The heat transfer coefficients are used to determine the amount of heat which is transferred and the energy distribution functions determine how this energy is distributed between various processes. The heat transfer regime selection is influenced strongly by flow regime; however, more than one heat transfer regime may exist in one flow regime. The selection of the wall heat transfer coefficients and energy distribution functions is dependent on the heat transfer regime maps. The flow regime maps determine the interphase and wall areas and the interphase heat transfer coefficient models. The heat transfer regimes considered, the method of selecting these regimes, and a description of how the energy partition functions are used are presented in this section. The heat transfer correlations are described in Section 6, and the energy partition functions are described in Section 7.

The wall heat transfer regimes modeled include:

1) free convection to a phase
2) forced convection to a phase
3) subcooled and saturated nucleate pool boiling
4) subcooled and saturated nucleate flow boiling
5) forced convection vaporization
6) transition and stable film pool boiling
7) transition and stable film flow boiling

5.1 Description of the Wall Heat Transfer Regimes

The method used to describe well known types of heat transfer in terms of the heat transfer regimes modeled is summarized in the following.

5.1.1 Single Phase Convection. Single phase free or forced convection is the basic heat transfer mode assumed unless other effects require that another heat transfer regime exists such as nucleate boiling. Free convection correlations are used for heat transfer in a phase when the velocity of that phase is effectively zero. Forced convection correlations are used otherwise. Free convection may be used in one phase and forced convection in the other as conditions warrant. In the present model, convection correlations rather than correlations particular to condensation are used when condensation occurs.

5.1.2 Subcooled and Saturated Nucleate Boiling. Nucleate boiling is characterized by a wall temperature greater than the saturation temperature. Subcooled boiling occurs when the average fluid temperature is less than the saturation temperature and saturated boiling occurs when the average fluid temperature is equal to the saturation temperature. A wall temperature greater than the saturation temperature implies that some of the liquid must be at saturation condition and, possibly, some at superheated liquid conditions. Liquid is in contact with the wall. Bubbles are formed at nucleation sites at the wall. When the bubbles are large enough, they detach from the wall and migrate into the liquid where they probably condense. Both nucleate pool and flow boiling are modeled with the former occurring when the velocity of the liquid is effectively zero. Nucleate boiling can occur in several flow regimes including separated flow. In separated flow, the vapor may be receiving heat by forced convection while the liquid in contact with the wall is experiencing nucleate boiling. Of course, many other situations are possible in separated flow and many of these are taken into account in the selection of the heat transfer regime.

5.1.3 Forced Convection Vaporization. This is a heat transfer regime associated with nucleate boiling in high void fraction annular flow. The heat transfer coefficient is convective in nature because it is strongly flow dependent. Nucleate boiling is assumed to be suppressed in this regime (Tong, 1965).

5.1.4 Transition Boiling. Transition boiling is a transition region between nucleate boiling and stable film boiling. Portions of the wall are wetted and alternately dried out in a random oscillating manner. These oscillations give rise to local fluctuations in the wall temperature.

5.1.5 Stable Film Boiling. Stable film boiling is characterized by the liquid not touching the wall due to a vapor film next to the wall. The liquid may be either continuous as in inverse annular flow, or discontinuous as in dispersed droplet flow. No special correlation is required to describe this region. The UVUT theory will describe this regime by free or forced convection to the vapor and a small contribution to the liquid with the transition boiling correlation.

5.1.6 Partial Nucleate Boiling. The transition region between convection and nucleate boiling is accounted for as the point where the nucleate boiling correlation gives a larger heat flux than the convection correlation. For simplicity a partial nucleate boiling correlation to represent the transition between these two regimes, as summarized in Tong (1965, p 113), is not used here. Future refinements could include such a correlation.

5.1.7 Condensation. Condensation does not require special correlations. It is represented with convection correlations. When a liquid film is formed on the wall as in annular flow, heat transfer from the liquid film is calculated by convection. Heat is transferred from the vapor to the liquid by appropriate interphase processes described in Section 6. When a dispersed flow regime is present, convection is assumed to account for heat transfer to both phases. Any liquid film which is formed by condensation is assumed to drain directly into the main body of the liquid.

Condensation is treated here in a much simpler manner than boiling because a complete parallelism does not occur between boiling and condensation. Dropwise condensation (nucleate condensation) is analogous to nucleate boiling and film condensation is analogous to film boiling. However, Merte (1973, p 227) pointed out that experimentally steam will condense dropwise on metal surfaces only under special conditions, with noble metals or special drop promoters. Film condensation, on the other hand, can occur spontaneously on most surfaces. Merte (1973, p 266) also pointed out that even when dropwise condensation occurs, no corresponding peak heat flux (departure from nucleate condensation) has been observed experimentally. Therefore, since only film condensation can occur, representation of condensation in terms of convection correlations is reasonable.

5.2 Method of Wall Heat Transfer Regime Selection

The method of selecting the wall heat transfer regime is shown in Figure (5.1). Selection criteria tests are based on the relation between the wall temperature and the phase temperatures, the volume fractions, the phase velocities, the magnitude of the heat flux, and the flow regime. This map is based on wall temperature (among other variables) as an input and wall heat flux as an output. Heat transfer between the wall and the fluid is characterized in two ways. The heat transfer rate per unit wall area (heat flux) is represented by $\dot{q}_w$, and the heat transfer rate per unit volume is represented by q_w. These heat transfer rates are related by

$$q_w = \bar{A}_w^q \dot{q}_w$$

where $\bar{A}_w^q$ is the wall area per unit volume available for heat transfer.

Initially, the wall temperature is compared to the saturation temperature. If the wall temperature is greater than the saturation temperature, then only free or forced convection can be occurring in any vapor that may exist. The test for free or

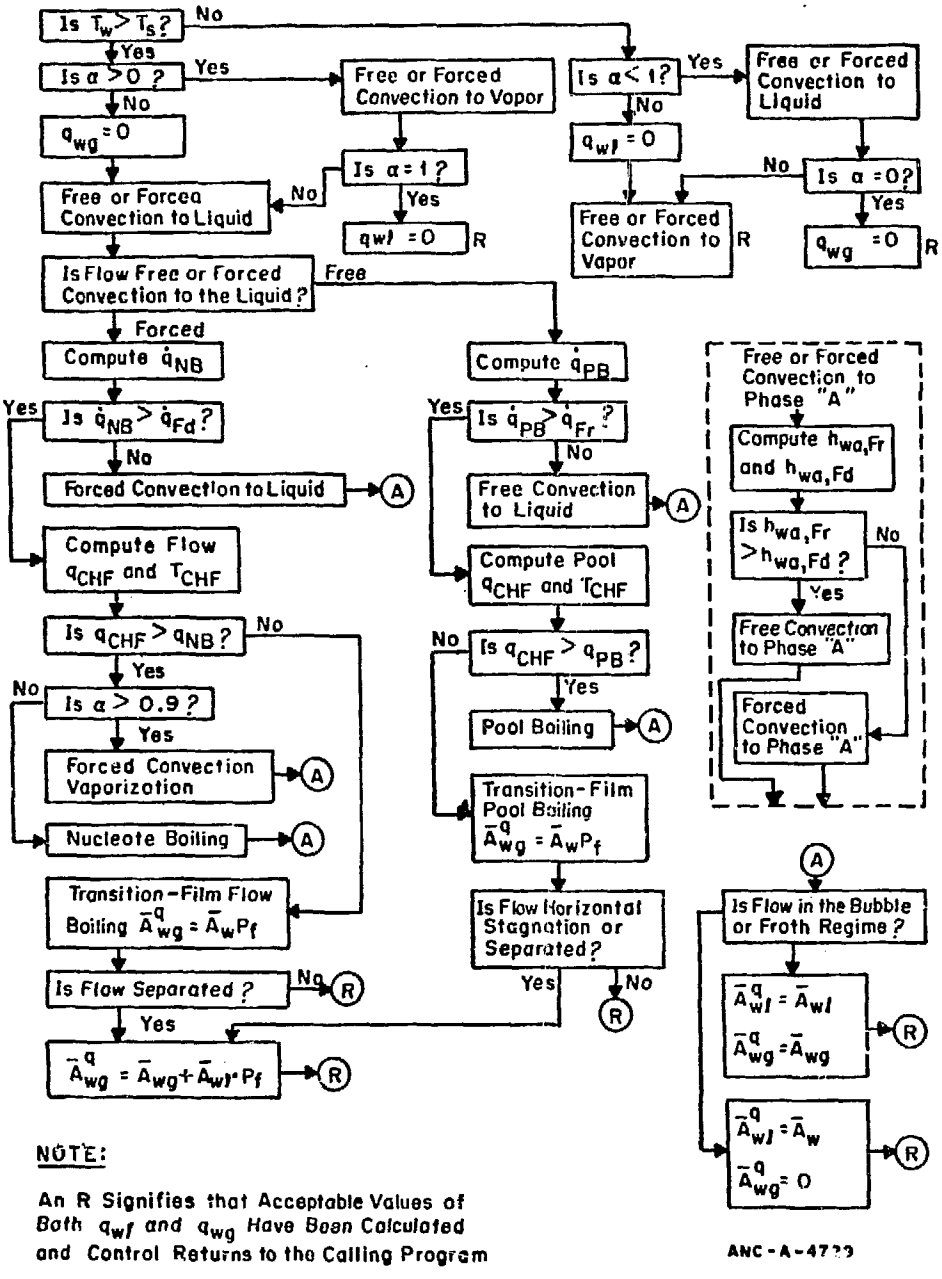

Figure 5.1 Wall Heat Transfer Regimes

forced convection to a phase is included in the insert in Figure (5.1). Heat transfer coefficients for free convection $h_{wa,Fr}$ and forced convection $h_{wa,Fd}$ are computed and the larger is selected. A free or forced convection test is then made for the liquid if any liquid exists. This test is used to determine which type of boiling (pool or flow) will be considered. The basis for the test for boiling is shown in Figure (5.2).

Both the convective (one phase liquid) and nucleate boiling heat fluxes are calculated for the given value of T_w. If the convective heat flux is greater than the nucleate boiling heat flux, one phase convective heat transfer is assumed. When the nucleate boiling heat flux is greater, the critical heat flux (CHF) is calculated and compared to the nucleate boiling heat flux. If the CHF value is greater than the nucleate boiling heat flux, nucleate boiling is assumed unless flow boiling occurs with $\alpha > 0.9$. When flow boiling occurs with $\alpha > 0.9$, bubble nucleation is assumed to be suppressed, and the wall heat transferred to the liquid is by forced convection vaporization. Although the correlation which is used was developed primarily from annular flow data, it is also applied in any flow regime which occurs when $T_s < T_w < T_{CHF}$ and $\alpha > 0.9$. The test for forced convection vaporization could be improved (Tong, 1965, p 119 and Hsu, 1962) but the current model is considered adequate for present purposes. Similarly, the transition between convective and nucleate boiling (partial nucleate boiling) could be improved (Tong, 1965, p 112) but the current model is considered adequate for present purposes.

The wall area available for heat transfer between the wall and each phase differs from the wall area for friction in some flow regimes. When the heat transfer is by convection to a single phase liquid, or by nucleate boiling in the bubble and froth flow regimes, the wall area per unit volume for heat transfer between the wall and each phase is

$$\bar{A}^{q}_{w\ell} = \bar{A}_w \tag{5.1}$$

$$\bar{A}^{q}_{wg} = 0 \quad . \tag{5.2}$$

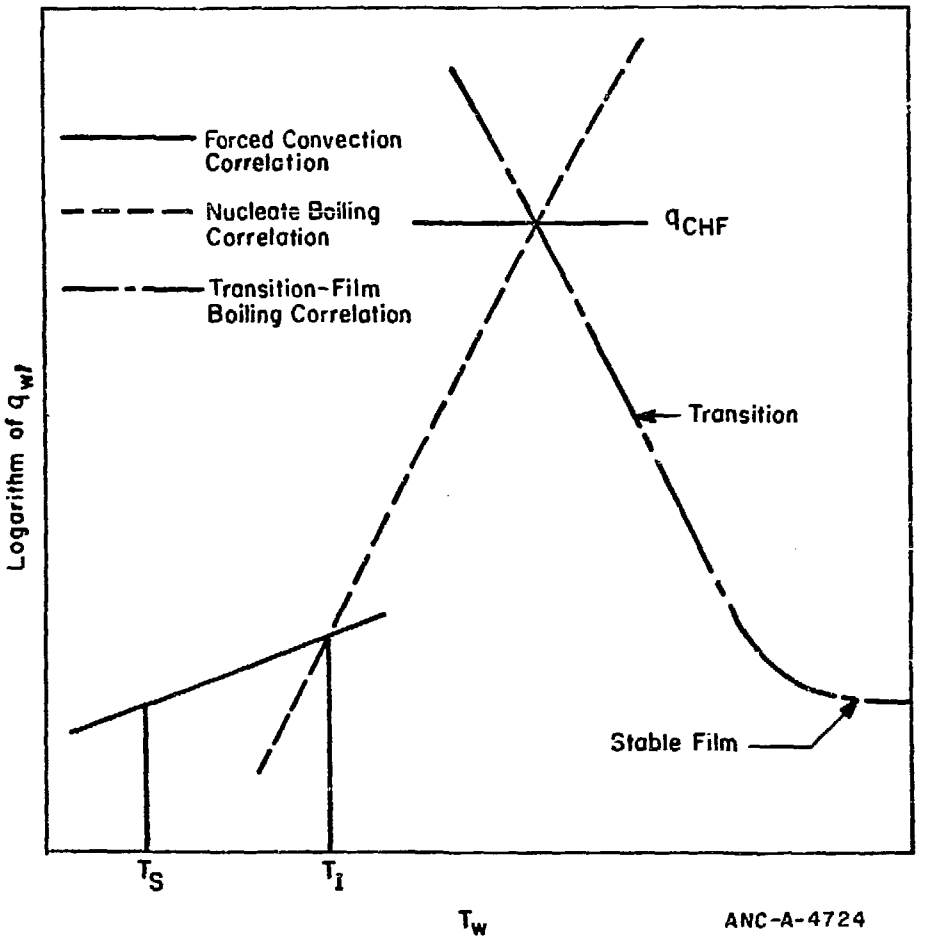

Figure 5.2 Selection of Liquid Heat Transfer Regime

In these regimes, a liquid layer is assumed to exist which covers the wall and is essentially stationary. This layer effectively insulates the vapor from the wall but provides an effective wall area to the vapor for resistance to flow. The nature of this liquid layer in nucleate boiling is related to the manner in which heat is transferred at nucleation sites. Bubbles are formed at nucleation sites but a superheated liquid layer separates the bubbles from the wall except for the area of the nucleation site itself (Snyder and Robin, 1968). The wall area exposed to the bubble is much smaller than the cross-sectional area of the bubble itself. Consequently, a small amount of area is exposed directly to the vapor which is neglected in the current model.

The wall heat transfer area model in Equations (5.1) and (5.2) is used for the annular and slug flow regimes but the wall areas for heat transfer in these regimes are the same as the wall areas for friction. In regimes for which the wall areas for heat transfer and friction differ, the heat flux to the vapor is recalculated when the heat transfer to the liquid is calculated. The separated flow regime is similar to the annular regime except that only the lower portion of the wall is available for nucleate boiling. The area for friction is, thus, the same as for heat transfer. The dispersed flow regime is considered to exhibit the process of convection or boiling in droplets on the wall when critical heat flux is not exceeded and the liquid coverage of the wall is limited to the cross-sectional area of the drop. The heat transfer wall areas used for this regime are consequently the same as the areas calculated for friction.

If the nucleate boiling heat flux is greater than the critical heat flux, transition or stable film boiling heat transfer is assumed. The transition-film boiling models in Section 6.1.7 describes heat transfer in both the transition and stable film boiling regimes. The stable film boiling regime as shown in Figure (5.2)

applies only to the heat transfer between the wall and the liquid phase, which does not increase with increasing wall temperature as does the total wall heat flux (Tong, 1965, p 2). The models described in Sections 6.1.6 and 6.1.7 compute a nonzero heat flux for the liquid phase in stable film flow boiling and a zero value in pool film flow boiling.

The wall heat transfer model for film boiling in the dispersed or inverse annular regime specifies that the gas phase covers the entire wall but does allow direct transfer of heat from the wall to the liquid even though the liquid does not touch the wall. The model acts as if the total wall area were available to both phases. The transition region is a combination of the critical heat flux and film boiling heat flux. This combination is made by use of a correlation which specifies the probability of nucleate boiling, P_N, and the probability of film boiling, P_F.*

$$P_N = \exp\left[- 0.693 \ (T_w - T_{CHF})\right] \tag{5.3}$$

and

$$P_F + P_N = 1. \tag{5.4}$$

The area for heat transfer to the gas phase is

$$\bar{A}^q_{wg} = \bar{A}_w \quad P_N \ . \tag{5.5}$$

Two areas are used for the heat transfer to the liquid, one for the nucleate boiling contribution

$$\bar{A}^q_{w\ell,NB} = \bar{A}_w \quad P_F \tag{5.6}$$

and one for the film boiling contribution

$$\bar{A}^q_{w\ell,FB} = \bar{A}_w \quad P_F \ . \tag{5.7}$$

*Personal communication, W. A. Yuill to J. A. McFadden, January 1974

At the current time, only inverse annular and dispersed flow can occur in the flow regime map for postcritical heat flux conditions. However, a provision is made for separated flow and the stagnant horizontal regime in the wall heat transfer regime map by correcting the wall areas for the amount of wall area which is exposed only to the vapor

$$\bar{A}^{q}_{wg} = \bar{A}_{wg} + \bar{A}_{w\ell} \quad P_F \tag{5.8}$$

$$\bar{A}^{q}_{w\ell,NB} = \bar{A}_{w\ell} \quad P_N \tag{5.9}$$

$$\bar{A}^{q}_{w\ell,FB} = \bar{A}_{w\ell} \quad P_F \, . \tag{5.10}$$

Finally, if the wall temperature is less than the saturation temperature, then only free or forced convection can occur in the liquid. Since no special correlations are used for condensation, free or forced convection is selected for the vapor also.

5.3 Relationship Between the Heat Transfer Mechanisms and Energy Partition Functions

In a two phase system with unequal phase temperatures, five heat transfer mechanisms (governed by the heat transfer coefficients) must be considered. To determine the proper distribution of mass and energy resulting from these processes Hocevar, et al., (1975) give a detailed description of the heat transfer mechanisms, the energy storage processes, and the use of the energy partition functions. This section summarizes the relationship between the heat transfer mechanisms and energy storage pressures.

5.3.1 Heat Transfer Mechanisms and Energy Storage Processes. The five heat transfer mechanisms considered in solving the UVUT equations which are governed by heat transfer coefficients are:

a) heat transfer to the liquid phase from a surface

b) heat transfer from the liquid phase to a surface

c) heat transfer to the vapor phase from a surface

d) heat transfer from the vapor phase to a surface

e) heat transfer from the vapor phase to the liquid phase

The energy transferred by these heat transfer mechanisms can produce either a temperature change or a phase change, depending on how the transferred energy is stored. The eight energy storage processes are:

1 heating of a subcooled liquid,

2 heating of a superheated vapor,

3 boiling of a liquid with an average liquid temperature less than the saturation temperature,

4 condensation of vapor with an average vapor temperature greater than the saturation temperature,

5 boiling of liquid with an average liquid temperature equal to saturation,

6 condensation of vapor with an average vapor temperature equal to saturation,

7 cooling of a superheated vapor, and

8 cooling of a subcooled liquid.

Convection, boiling, and condensation processes result by combining the heat transfer mechanisms and energy storage processes. Mechanism "a" and process "1" represent convection from a surface to a liquid. Boiling of a subcooled liquid by a vapor is represented by mechanism "e" and processes, "1", "3", and "6".

The heat transfer mechanisms can result in mass exchange, depending on which energy storage process is involved. The rate at which mass is produced in such a process can be computed by dividing the heat transfer rate by the heat of vaporization.

The various combinations of heat transfer mechanisms and energy storage processes, including the mass exchange processes, are summarized in Figure (5.3).

5.3.2 Use of Energy Partition Functions. The energy partition functions are used to determine the energy distribution when two energy storage processes are possible. An example is boiling of a subcooled liquid. Part of the energy transferred from the surface to the liquid goes to heating the liquid, q_{a1}, and part goes to vaporization, q_{a3}. If the total heat transferred to the liquid is $q_{w\ell}$, and F_{a3} is the fraction of this energy which is used in vaporization, then

$$q_{a1} = (1 - F_{a3})\, q_{w\ell} \tag{5.11}$$

and

$$q_{a3} = F_{a3}\, q_{w\ell} . \tag{5.12}$$

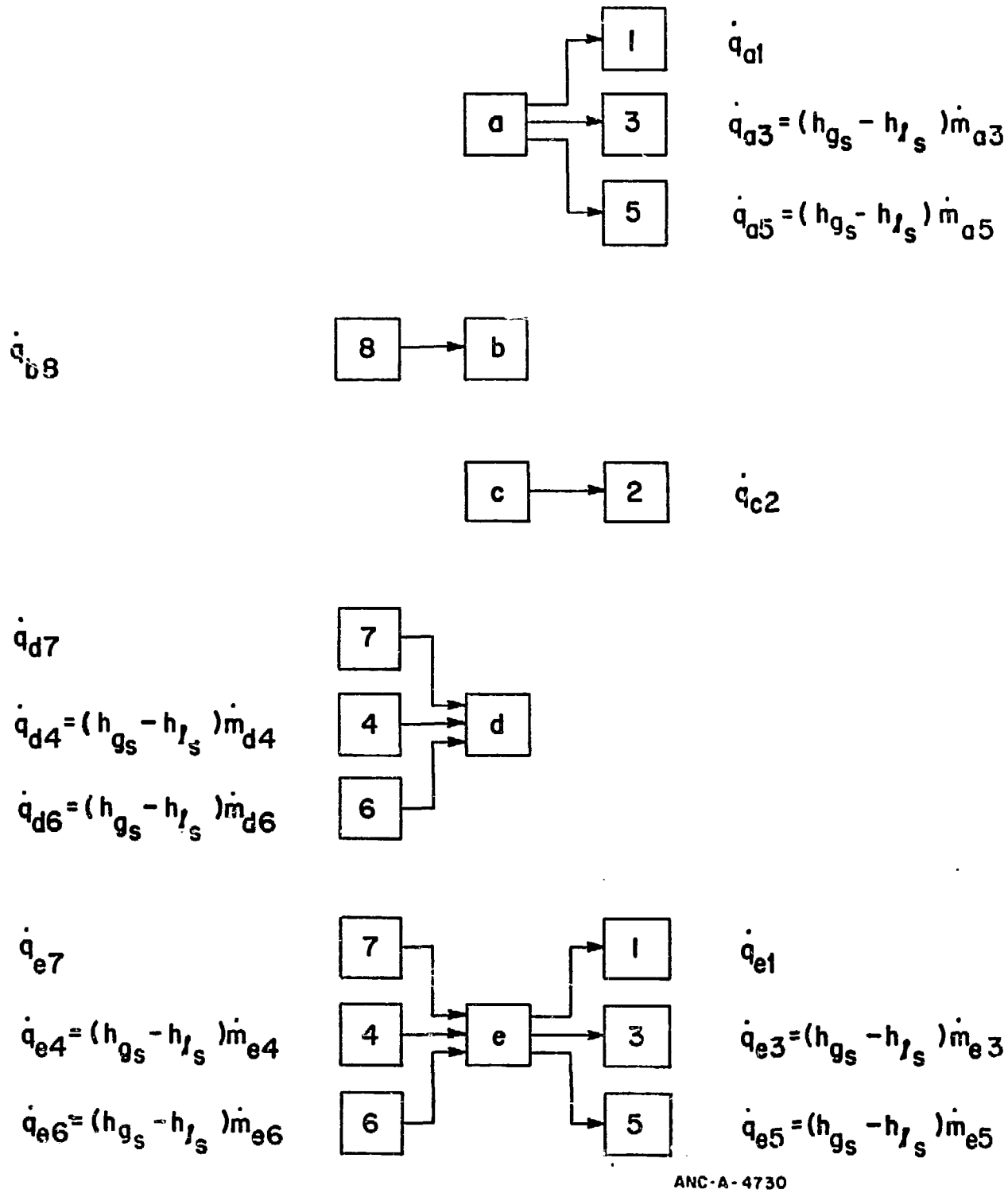

Figure 5.3 Possible Heat Transfer Mechanisms and Energy Storage Combinations

Three other energy partition functions are required. Heat can be transferred from a superheated vapor to a surface by cooling or condensation of the vapor F_{d4} is the energy partition function which determines the fraction of the energy which goes into condensation.

The other two partition functions are associated with heat transfer mechanism "e" which is heat transfer from the vapor phase to the liquid phase. These functions are F_{e3} and F_{e4} and their use is analogous to F_{a3} and F_{d4}.

Energy partition functions are also used to determine the amount of fluid at saturation conditions when the entire fluid is not at saturation conditions. This information is required in order to describe the interphase heat and mass transfer which occurs due to depressurization. For example, the mass partition function (ratio of liquid at saturation to total liquid), for subcooled liquid can be directly related to the appropriate energy distribution functions.

The assumption is made that the mass of the liquid can be subdivided into portions affected by the wall, $m_{\ell_{wall}}$, and by the other phase, $m_{\ell_{vap}}$ as

$$m_{\ell} = m_{\ell_{wall}} + m_{\ell_{vap}} . \tag{5.13}$$

A similar relation holds for the vapor. The energy partition function for a liquid, with an average temperature less than the saturation temperature in contact with a wall specifies the split of heat which goes into latent and sensible heat. This split may be interpreted as being due to the relative

amount of liquid which is at saturation and which is truly subcooled. This interpretation implies that the mass partition functions are equal to the energy partition functions. Thus the amount of mass at saturation conditions due the wall, $m_{\ell_{\substack{wall \\ sat}}}$, and due to the vapor, $m_{\ell_{\substack{vap \\ sat}}}$, is

$$m_{\ell_{\substack{wall \\ sat}}} = F_{a3}\, m_{\ell_{wall}} \tag{5.14}$$

$$m_{\ell_{\substack{vap \\ sat}}} = F_{e3}\, m_{\ell_{vap}} . \tag{5.15}$$

The total mass of liquid which is saturated is given by

$$m_{\ell_{sat}} = m_{\ell_{\substack{wall \\ sat}}} + m_{\ell_{\substack{vap \\ sat}}} . \tag{5.16}$$

The total fraction of the liquid which is saturated can be determined by combining Equations (5.13) through (5.16)

$$\frac{m_{\ell_{sat}}}{m_{\ell}} = \frac{F_{a3}\, m_{\ell_{wall}} + F_{e3}\, m_{\ell_{vap}}}{m_{\ell_{wall}} + m_{\ell_{vap}}} . \tag{5.17}$$

The mass of the liquid which is affected by the wall and the vapor will be assumed to be proportional to the heat transfer areas between the liquid and wall, $\bar{A}^{q}_{w\ell}$, and the liquid and vapor, $\bar{A}^{q}_{g\ell}$

$$\frac{m_{\ell_{wall}}}{m_{\ell}} = \left(\frac{\bar{A}^{q}_{w\ell}}{\bar{A}^{q}_{w\ell} + \bar{A}^{q}_{g\ell}}\right) . \tag{5.18}$$

$$\frac{m_{\ell_{vap}}}{m} = \left(\frac{\bar{A}^{q}_{g\ell}}{\bar{A}^{q}_{w\ell} + \bar{A}^{q}_{g\ell}}\right) \tag{5.19}$$

In the limit, the fraction of liquid at saturation will be unity when the energy partition functions are unity. The mass of vapor at saturation is determined in the same manner.

Other models could also have been considered. For example, the energy partition functions used to determine the fraction of the masses that are saturated could be different than those used to determine the energy split. Experimental data might show that Equations (5.18) and (5.19) should be modified for different flow regimes.

The heat transfer coefficients and energy partition functions used are described in the following two sections.

6. HEAT TRANSFER COEFFICIENTS

In the UVUT equations, the energy per unit volume transferred between a surface and the liquid phase, $q_{w\ell}$, and a surface and the vapor phase, q_{wg}, and the interphase energy exchange, $q_{g\ell}$, must be determined. The rate of energy exchange per unit volume between a surface and the fluid is

$$q_w = q_{w\ell} + q_{wg} \tag{6.1}$$

where

$$q_w = (\bar{A}_{w\ell} + \bar{A}_{wg})\, \dot{q}_w, \tag{6.2}$$

$$q_{w\ell} = \bar{A}^{q}_{w\ell}\, h_{w\ell}\, (T_w - T_\ell), \tag{6.3}$$

$$q_{wg} = \bar{A}^{q}_{wg}\, h_{wg}\, (T_w - T_g)\ . \tag{6.4}$$

$h_{w\ell}$ = heat transfer coefficient between the wall and the liquid

and

h_{wg} = heat transfer coefficient between the wall and the vapor.

The interphase energy transfer rate per unit volume is

$$q_{g\ell} = \bar{A}^{q}_{g\ell}\, h_{g\ell}\, (T_g - T_\ell) \tag{6.5}$$

where

$h_{g\ell}$ = heat transfer coefficient between the gas and liquid phase.

The correlations used to determine the heat transfer rates are described in this section.

6.1 Wall to Phase Heat Transfer

The correlations used for heat transfer between the wall and a phase for all wall heat transfer regimes are discussed in the following.

6.1.1 Single Phase Free Convection. The heat transfer coefficient for free convection is computed from the correlation (Jacob and Hawkins, 1947, p 128).

$$\frac{h_{wa} D}{k_a} = 0.135 \left[\left(\frac{\beta g (T_w - T_a)\, D^3 \rho_a^2}{\mu_a^2} \right) \left(\frac{c_p \mu}{k} \right)_a \right]^{1/3} \tag{6.6}$$

where β = coefficient of linear expansion of the surface material

c_p = specific heat

k = thermal conductivity

h_{wa} = wall to phase "a" heat transfer coefficient

and g = gravitational constant.

This correlation is an average between a correlation from vertical plates and cylinders (for which the coefficient is 0.13) and a correlation for heat transfer from hot plates facing upward or cooled plates facing downward (for which the coefficient is 0.14). This expression is valid for turbulent free convection and is a reasonable approximation for laminar free convection.

The wall to phase heat transfer rate per unit volume is

$$q_{wa} = A^q_{wa} \, h_{wa} \, (T_w - T_a) \quad . \tag{6.7}$$

In the bubble or froth flow regime when $T_w > T_s$,

$$\bar{A}^q_{wg} = 0$$

$$\bar{A}^q_{w\ell} = \bar{A}_w \quad .$$

In all other regimes, the wall area for heat transfer is the same as the wall area for friction.

6.1.2 Single Phase Forced Convection Correlations for forced convection heat transfer to single phase fluids were reviewed. Although most of these correlations showed negligible differences for heat transfer to water, significant deviations result when they are applied to heat transfer to high pressure, superheated steam. Forced convection heat transfer to both subcooled water and superheated steam appears to be best correlated by the Colburn (1933) equation,

$$\left(\frac{h_{wa}}{c_{pb} G}\right)_a \left(\frac{c_p \mu}{k}\right)^{0.66}_{fa} = 0.023 \left(\frac{DG}{\mu_f}\right)^{-0.2}_a \quad . \tag{6.8}$$

Subscript "b" refers to properties evaluated at the bulk temperature of the fluid and subscript "f" refers to properties evaluated at the film temperature, T_f, given by

$$T_f = \frac{1}{2}(T_w + T_b)$$

Equation (6.8) can be rearranged in the form

$$\left(\frac{hD}{k_f}\right)_a = 0.023\left(\frac{DG}{\mu_f}\right)_a^{0.8}\left(\frac{c_p\mu}{k}\right)_{fa}^{0.33}\left(\frac{c_{pb}}{c_{pf}}\right)_a . \qquad (6.9)$$

This equation is the Dittus-Boelter equation (Dittus and Boelter, 1930) with three exceptions. The Dittus-Boelter equation is evaluated in terms of bulk properties and a value of 0.4 instead of 0.33 is used as an exponent of the Prandtl number, $c_p\mu/k$. The same model is used to compute q_{wa} from h_{wa} as in free convection.

6.1.3 Subcooled and Saturated Nucleate Pool Boiling This regime can only occur when $T_w > T_s$. The correlation of Rohsenow (Rohsenow, 1952 and Frost and Li, 1971) is used to determine heat transfer to the liquid for nucleate pool boiling. This correlation is

$$\frac{c_{p\ell}(T_w-T_s)}{h_{fg}} = C_{sf}\left[\frac{\dot{q}_w}{\mu_\ell h_{fg}}\left(\frac{\sigma}{\rho_\ell-\rho_g}\right)^{1/2}\right]^{1/3}\left(\frac{\mu_\ell c_{p\ell}}{k_\ell}\right) . \qquad (6.10)$$

The coefficient C_{sf} depends on the surface-fluid combination, and is taken as 0.013 (Collier, 1972 p 124). This equation may be solved for $\dot{q}_w$ as

$$\dot{q}_w = \frac{k_\ell^3}{(C_{sf})^3}\,\frac{(T_w-T_s)^3}{\mu_\ell^2 h_{fg}^2}\left(\frac{\rho_\ell-\rho_g}{\sigma}\right)^{1/2} . \qquad (6.11)$$

The volumetric heat flux to each phase for bubble and froth flows is

$$q_{w\ell} = \bar{A}_w \dot{q}_w \qquad (6.12)$$

and

$$q_{wg} = 0 . \qquad (6.13)$$

In all other flow regimes

$$q_{w\ell} = \bar{A}_{w\ell} \dot{q}_w \qquad (6.14)$$

and

$$q_{wg} = \bar{A}_{wg} h_{wg} (T_w - T_g) \qquad (6.15)$$

where h_{wg} is the appropriate convection coefficient.

6.1.4 Subcooled and Saturated Nucleate Flow Boiling The Thom (Thom et al., 1966) correlation is used to compute the heat transfer coefficient from the wall to the fluid during subcooled and saturated flow nucleate boiling. This correlation is

$$\dot{q}_w = \left[\frac{(T_w - T_s)\, e^{P/1260}}{4.32} \right]^2 \tag{6.16}$$

where P = local pressure, psia.

The heat transfer to each phase is calculated in the same manner as in nucleate pool boiling. At present, saturated nucleate boiling is treated the same as subcooled nucleate boiling, with the only difference being that the liquid is at the saturation temperature.

6.1.5 Forced Convection Vaporization In the case of annular flow with $\alpha > 0.9$ wall heat transfer is assumed to occur by a forced convection-vaporization mechanism. In forced convection-vaporization, nucleate boiling in the liquid film is suppressed and energy transfer from the wall is by forced convection in the liquid film, with vaporization occurring at the film-vapor core interface. The Schrock-Grossman (1957) correlation is used to compute an overall heat transfer coefficient, h_w in the following:

$$h_w \cdot \quad Nu = (2.50)\ (0.023)\ Pr_\ell^{0.4} \left[\frac{GD^\ell{}_w(1-x')}{\mu_\ell} \right]^{0.8} \left[\frac{1}{X_{tt}} \right]^{0.75} \tag{6.17}$$

where

$$Nu = \frac{h_{w\ell} D^\ell{}_w}{k_\ell} \tag{6.18}$$

$$x' = \alpha\rho_g v^g / (\alpha\rho_g v^g + (1-\alpha)\rho_\ell v^\ell) \tag{6.19}$$

$$G = \alpha\rho_g v^g + (1-\alpha)\rho_\ell v^\ell$$

$$\frac{1}{X_{tt}} = \left(\frac{x'}{1-x'}\right)^{0.9}\left(\frac{\rho_\ell}{\rho_g}\right)^{0.5}\left(\frac{\mu_g}{\mu_\ell}\right)^{0.1} \qquad (6.20)$$

Substitution of $1/X_{tt}$ into Equation (6.20) yields

$$Nu = (2.5)\ (0.023)\ Pr_\ell^{0.4}\left[\frac{GD_w^\ell}{\mu_\ell}\right]^{0.8}(1-x')^{0.125}(x')^{0.675}\left(\frac{\rho_\ell}{\rho_g}\right)^{0.375}\left(\frac{\mu_g}{\mu_\ell}\right)^{0.075} \qquad (6.21)$$

This expression is well behaved at $\alpha = 1$. The wall heat flux is

$$\dot{q}_w = h_w\ (T_w - T_\ell)$$

The wall heat flux per unit volume to each phase is calculated in the same manner as for nucleate boiling.

6.1.6 Transition and Stable Film Pool Boiling The transition boiling regime is described by the combination of the heat flux at critical heat flux and the heat transfer to the liquid in stable film boiling. In pool boiling, the heat transfer directly to the liquid in stable film boiling is assumed to be zero. The heat transfer to each phase is given by

$$q_{wg} = \bar{A}^q_{wg}\ h_{wg}\ (T_w - T_g) \qquad (6.22)$$

where h_{wg} is the appropriate convection coefficient and

$$q_{w\ell} = \bar{A}^q_{w\ell,NB}\ \dot{q}_{CHF} \qquad (6.23)$$

Equations (5.3) through (5.10) are used to compute the area terms.

6.1.7 Transition and Stable Film Flow Boiling A model was developed to calculate heat transfer to the liquid phase in stable film boiling. This model uses the Reynolds flux analogy (Wallis, 1968) to compute the flux of liquid to the wall. The model assumes that the droplets approaching the wall are repulsed by the vapor generated on the portion of the droplet facing the wall.

To extend this model to account for heat transfer between the wall and the liquid in the transition boiling regime, a weighted combination of the wall to liquid heat transfer rates for the CHF and stable film boiling conditions is used. The weighting factors are related to the probability of the liquid wetting the wall [equation (5.3)]. The expression for the heat flux to the liquid phase is

$$\dot{q}_{w\ell} = \frac{(1-\alpha)\, f_\ell \rho_\ell |v^\ell|}{8} \left[\frac{|v^\ell|}{\bar{v}_r} P_F + P_N \exp\left(- \frac{\dot{q}_{w\ell}}{h_{fg} 2\varepsilon_o} \sqrt{\frac{\rho_m}{\rho_g}} \right) \right] \left(h_{gs} - h_\ell \right) \quad (6.24a)$$

where

$\bar{v}_r$ = molecular velocity of the liquid normal to the wall,

$$\varepsilon_o = \frac{f_\ell}{2} \rho_m |v^\ell|$$

and

ρ_m = mixture density.

The molecular velocity

$$\bar{v}_r = \sqrt{\frac{2kT_\ell}{\pi m}}$$

is associated with the molecules leaving the liquid surface, where

k = Boltzman constant

m = Molecular weight

Equation (6.24) could be solved iteratively for $\dot{q}_{w\ell}$. The present model in UVUT approximates $\dot{q}_{w\ell}$ in the exponent on the right hand side of Equation (6.24) by the critical heat flux. This approximation will result in a slight but not serious, underestimation of the nucleate boiling contribution to the total liquid heat flux. The heat transfer rate to the liquid phase per unit volume then is

$$q_{w\ell} = \frac{(1-\alpha)\, f_\ell \rho_\ell |v^\ell|}{8} \left[\frac{|v^\ell|}{\bar{v}_r} \bar{A}^q_{w\ell,FB} + \bar{A}^q_{w\ell,NB} \exp\left(- \frac{\dot{q}_{CHF}}{2\varepsilon_o h_{fg}} \sqrt{\frac{\rho_m}{\rho_g}} \right) \right] \left(h_{gs} - h_\ell \right) \quad (6.24b)$$

The coefficient for heat transfer between the wall and the vapor is computed from Equation (6.8) and the wall area terms are calculated by Equations (5.3) through (5.10).

6.2 Interphase Heat Transfer

To compute heat transfer between phases at unequal temperatures, four heat transfer mechanisms must be considered. These mechanisms are

1. Conduction within the liquid (vapor)
2. Condensation of vapor on the surface of the liquid
3. Convection of sensible heat to the surface of liquid (vapor)
4. Evaporation of liquid from the liquid surface.

The net interphase heat transfer can be computed by modelling just two of these mechanisms, conduction and convection. To illustrate this modelling the case of a subcooled drop in a superheated vapor is considered.

When the drop is placed in the vapor, the temperature at the surface of the drop rapidly approaches the saturation temperature. Conduction heat transfer will continue to dominate until the temperature profile in the drop is such that convection of heat in the vapor to the surface of the drop equals conduction of heat in the drop. As the drop continues to warm ($T_\ell \rightarrow T_s$), convection in the vapor becomes the dominant form of interphase heat transfer. Condensation and vaporization occur when convection and conduction modes of heat transfer are unequal. If conduction from the surface of the drop to the interior is greater than convection from the vapor to the drop surface, condensation will occur. If the convection heat transfer is greater than the conduction heat transfer, vaporization will result.

A similar discussion could be presented for a superheated vapor bubble in a continuous liquid phase.

The interphase heat transfer is dependent on the interphase geometry, so the interphase heat transfer models are given for the flow regimes discussed in Section 2.1. The nomenclature for the heat transfer coefficients and heat fluxes is described in Section 5.3.

6.2.1 Bubble, Froth and Vertical Stagnation Regimes For these flow regimes, the vapor phase is in the form of bubbles with radius r_p. The heat transfer rate due to convection in the liquid phase is computed from the rate at which the bubble collapses (Moalem and Sideman, 1973). The heat flux at the bubble surface can be related to the rate of bubble collapse. The resulting heat transfer coefficient for convection in the liquid is

$$h_{el} = k_\ell \left[\frac{2 \left| v^\ell - v^g \right| 0.25 \, Pr_\ell^{-0.33}}{\pi a_\ell r_p} \right]^{1/2} \tag{6.25}$$

where a_ℓ is the thermal diffusivity for the liquid phase,

$$a_\ell = \frac{k_\ell}{\rho_\ell c_{p\ell}} \tag{6.26}$$

The heat transfer rate is

$$\dot{q}_{el} = h_{el} (T_s - T_\ell) \tag{6.27}$$

The heat transfer due to conduction in the bubble is based on approximating the time dependent heat transfer by a time independent solution. The resulting heat transfer coefficient is

$$h_{e7} = 8.067 \frac{k_g}{r_p} \tag{6.28}$$

and the heat transfer rate is

$$\dot{q}_{e7} = h_{e7}(T_g - T_s) . \tag{6.29}$$

The interphase heat transfer rate, $\dot{q}_{g\ell}$, is the maximum of the values given by Equations (6.27) and (6.29). If $\dot{q}_{e7}$ is greater than $\dot{q}_{e1}$, the amount of heat which goes into boiling is $\dot{q}_{e7} - \dot{q}_{e1}$ and if $\dot{q}_{e1}$ is larger, the amount of heat obtained from condensation is $\dot{q}_{e1} - \dot{q}_{e7}$.

6.2.2 Annular, Slug and Countercurrent (Liquid on Wall) Regimes In the present UVUT model all the liquid is assumed to be found in an annular film for these flow regimes. Thus, the interphase heat transfer occurs only at the liquid film–vapor core interface.

The heat transfer coefficient for conduction in the liquid film is

$$h_{e1} = \frac{k_\ell}{\delta_\ell} \tag{6.30}$$

where δ_ℓ is the film thickness, which is

$$\delta_\ell = R - R_i = \frac{D}{2}(1 - \sqrt{\alpha}) . \tag{6.31}$$

The heat flux in the liquid due to conduction is

$$\dot{q}_{e1} = h_{e1}(T_s - T_\ell) . \tag{6.32}$$

The heat transfer coefficient due to convection in the gas center core is computed from the Dittus–Boelter (1930) correlation,

$$Nu = 0.023\ Re^{0.8}\ Pr^{0.4} \tag{6.33}$$

where for the case of annular flow

$$Nu = \frac{h_{e7}\ 2(R-\delta_\ell)}{k_g} \tag{6.34}$$

$$Re = \frac{\rho_g \left| v^\ell - v^g \right| 2(R-\delta_\ell)}{\mu_g} \ . \tag{6.35}$$

The interphase heat flux due to convection is

$$\dot{q}_{e7} = h_{e7}\ (T_g - T_s) \tag{6.36}$$

and the net interphase heat transfer is given by the maximum of the values from Equations (6.32) and (6.35) with the amount of energy going into phase change calculated as in the previous case.

6.2.3 Dispersed Regime In the dispersed flow regime, the interphase heat transfer occurs between the continuous vapor phase and the droplets of radius, r_p. The heat transfer coefficient for conduction to the liquid droplets, h_{e1}, is analagous to Equation (6.28) and is given by

$$h_{e1} = 8.067\ \frac{k_\ell}{r_p} \tag{6.37}$$

and the heat transfer rate is

$$\dot{q}_{e1} = h_{e1}\ (T_s - T_\ell) \ . \tag{6.38}$$

The heat transfer coefficient for convection, h_{e7}, in the continuous gas phase is the Frossling equation as given by Fuchs (1959),

$$Nu = 2(1 + \beta\, Re^{0.5}\, Pr_g^{0.33}) \tag{6.39}$$

or

$$h_{e7} = \frac{1}{r_p}\left[1 + \beta\, Re^{0.5}\, Pr_g^{0.33}\right] \tag{6.40}$$

where $\beta = 0.37$

$$Re = \frac{2\rho_g \left| v^{\ell} - v^{g} \right| r_p}{\mu_g} \tag{6.41}$$

The heat transfer rate for convection then is

$$\dot{q}_{e7} = h_{e7}\,(T_g - T_s) \tag{6.42}$$

The interphase heat transfer, $q_{g\ell}$, is the maximum of the values given by Equations (6.38) and (6.42). If $\dot{q}_{e7}$ is greater than $\dot{q}_{e1}$, the amount of heat which goes into boiling is $\dot{q}_{e7} - \dot{q}_{e1}$ and, if $\dot{q}_{e1}$ is larger, the amount of heat obtained from condensation is $\dot{q}_{e1} - \dot{q}_{e7}$.

6.2.4 Inverse Annular and Countercurrent (Vapor on Wall) Regimes The interphase heat transfer for these flow regimes is determined by considering conduction in the vapor film (radiation is neglected) and convection in the center liquid core.

The heat transfer coefficient due to conduction in the vapor film is

$$h_{e7} = \frac{k_g}{\delta_g} \tag{6.43}$$

where δ_g, the vapor film thickness, is computed from Equation (3.23) as

$$\delta_g = R(1 - \sqrt{1-\alpha}) = \frac{D}{2}(1-\sqrt{1-\alpha}) \quad (6.44)$$

The heat flux due to conduction is

$$\dot{q}_{e7} = h_{e7}(T_g - T_s). \quad (6.45)$$

The heat transfer coefficient for convection in the liquid is determined from the Dittus - Boelter (1930) correlation,

$$Nu = 0.023\, Re^{0.8}\, Pr_\ell^{\,0.4} \quad (6.46)$$

where

$$Nu = \frac{h_{e1}\, 2\,(R-\delta_g)}{k_\ell} \quad (6.47)$$

$$Re = \frac{\rho_\ell \left| v^\ell - v^* \right| 2(R-\delta_g)}{\mu_\ell} \quad (6.48)$$

The interphase heat flux due to convection is

$$\dot{q}_{e1} = h_{e1}(T_s - T_\ell) \quad (6.49)$$

and the net interphase heat transfer is computed as discussed in Section 6.2.1

6.2.5 Separated and Horizontal Stagnation Regimes In the separated and horizontal stagnation flow regimes, convection will be the primary mode of heat transfer in both phases except for very small and very large values of the vapor volume fraction. If the interface is at the saturation temperature, net condensation or evaporation can be determined as in the previous sections.

The convection heat transfer coefficient for the liquid phase is computed from the Dittus - Boelter (1930) equation,

$$Nu = 0.023\ Re_{\ell}^{0.8}\ Pr_{\ell}^{0.4} \tag{6.50}$$

where

$$Nu = \frac{h_{e1}\ D_{int}^{\ell}}{k_{\ell}} \tag{6.51}$$

and

$$D_{int}^{\ell} = \frac{2\pi R\ (1-2\alpha)}{Sin\ \frac{\theta}{2} + \pi - \frac{\theta}{2}} \tag{6.52}$$

and the Reynolds number is given by Equation (3.44).

The convection heat transfer coefficient of the vapor phase is computed from

$$Nu = 0.023\ Re_{g}^{0.8}\ Pr_{g}^{0.4} \tag{6.53}$$

with

$$Nu = \frac{h_{e7}\ D_{int}^{g}}{k_{g}} \tag{6.54}$$

and D_{int}^{g} computed from Equation (3.66) and Re_{g} computed from Equation (3.44).

The interphase heat fluxes are

$$\dot{q}_{e1} = h_{e1}\ (T_s - T_{\ell}) \tag{6.55}$$

and

$$\dot{q}_{e7} = h_{e7}\ (T_g - T_s)\ . \tag{6.56}$$

The net interphase heat transfer is computed the same as for the other flow regimes.

6.3 Critical Heat Flux

Critical heat flux correlations for both pool and forced convective boiling are required to determine both heat transfer and flow regimes. The CHF correlations presently used in UVUT are discussed in this section.

6.3.1 Critical Heat Flux in Pool Boiling The CHF correlation for saturated pool boiling is based on the correlation of Kutateladze (1952). This correlation is obtained by determining the flux of vapor from the heated surface which is sufficient to keep the liquid phase from reaching the surface. Zuber (Tong, 1972, p 52) verified this correlation with a theoretical analysis based on the postulate that a pool boiling crisis is caused by a Helmholtz instability at the interface of a counterflow of two immiscible fluids. Zuber's correlation is

$$\dot{q}_{CHF,SAT} = 0.16\, h_{fg} \sqrt{\rho_g}[\sigma g(\rho_\ell - \rho_g)]^{1/4} \left[\frac{\rho_\ell}{\rho_\ell + \rho_g}\right]^{1/2} \tag{6.57}$$

This correlation reduces to the Kutateladze form when $\rho_\ell >> \rho_g$. For a subcooled liquid, the critical heat flux had been correlated by Ivey and Morris (1962, 1965) as

$$\frac{\dot{q}_{CHF}}{\dot{q}_{CHF,SAT}} = \left[1 + 0.1\left(\frac{\rho_\ell}{\rho_g}\right)^{0.75}\left(\frac{c_{p\ell}}{h_{fg}}\right)(T_s - T_\ell)\right] \tag{6.58}$$

The combination of correlations (6.57) and (6.58) is used here for both subcooled and saturated pool boiling CHF.

The flow regime selection logic, Figure 2.1, requires the wall temperature corresponding to critical heat flux. This temperature is obtained by substituting the value of $\dot{q}_{CHF}$ calculated by Equation (6.58) into the Rohsenow correlation [Equation (6.10)] and solving for T_{CHF}.

6.3.2 Critical Heat Flux in Flow Boiling The critical heat flux correlation used in UVUT is based on a model developed by Yuill and Mills (1973). This model was derived by considering that CHF occurs when the wall heat flux is just sufficient to vaporize all the liquid in contact with the wall. The Reynolds flux model (Wallis, 1968) is used to compute the mass flux of the liquid to the wall.

The equation for the critical heat flux is

$$\dot{q}_{CHF} = \frac{(1-\alpha)\rho_\ell f_\ell |v^\ell|}{8} \exp\left[\frac{\dot{m}}{2\epsilon_o}\sqrt{\frac{\rho_m}{\rho_g}}\right]\left[h_{fg} + c_{p\ell}(T_s - T_\ell)\right] \qquad (6.59)$$

where

f = Moody friction factor

$\dot{m}$ = mass flux of vapor from the wall

$\epsilon_o = \frac{f_\ell}{2}\rho_m |v^\ell|$

ρ_m = mixture density .

At the critical heat flux condition, all the liquid reaching the wall is vaporized, and leaves the wall with a mass flux of $\dot{m}$. This condition is expressed as

$$\dot{q}_{CHF} = \dot{m}\, h_{fg} \ . \qquad (6.60)$$

To compute the CHF value, Equation (6.60) is solved for $\dot{m}$ and sustituted into Equation (6.59). The resulting equation is solved using a Newton - Raphson method, with the initial estimate of q_{CHF} being the present value of the wall heat flux.

To determine the temperature corresponding to critical heat flux for use in the flow regime map, the Thom correlation [Equation (6.16)] is solved inversely for $T_w = T_{CHF}$,

$$T_{CHF} = T_s + 4.32\,(\dot{q}_{CHF})^{0.5}\, e^{-P/1260} \ . \qquad (6.61)$$

7. ENERGY PARTITION FUNCTIONS

As mentioned previously in Section 5.3, the energy partition functions are used to partition the energy which is calculated to occur due to heat transfer coefficients between competing energy storage processes. A set of prototype energy partition functions was used in the SVUT code by Hocevar, et al (1975). These functions were not based upon physical models but were developed only to produce reasonable results from the SVUT code. The models presented here are based on physical models and represent an improvement over the prototype models. Restrictions are placed on all energy partition functions in order to restrict physically unrealistic events from occurring such as the complete disappearance of a subcooled liquid below saturation. The four required energy partition functions are described in this section and compared to the appropriate restrictions.

7.1 Surface to Liquid Heat Transfer - All Heat Transfer Regimes

The energy partition function for subcooled boiling associated with a wall is the ratio of the amount of energy which goes into subcooled boiling to the total amount of heat transferred from the wall to the liquid,

$$F_{a3} = \frac{q_{a3}}{q_{w\ell}} . \tag{7.1}$$

The amount of energy going into subcooled boiling is the difference between the total heat transferred to the liquid and the amount convected and conducted into the liquid and is given by

$$q_{a3} = q_{w\ell} - a_C \bar{A}_{w\ell} (T_s - T_\ell) \tag{7.2}$$

where h_c is the appropriate free or forced convection heat transfer coefficient for the liquid phase as determined in Section 6.1.1 or Section 6.1.2. The energy partition function is

$$F_{a3} = 1 - \frac{h_c \bar{A}_{w\ell} (T_s - T_\ell)}{q_{w\ell}} \tag{7.3}$$

The only reason that the energy partition function is needed in this application is to make certain that the restrictions inherent in the nonequilibrium process of subcooled boiling are satisfied. The value of q_{a3} can be used directly in application, if desired. Since $q_{w\ell} = h_{w\ell} \bar{A}_{w\ell} (T_w - T_\ell)$, the energy distribution can be expressed as

$$F_{a3} = 1 - \frac{h_c (T_s - T_\ell)}{h_{w\ell} (T_w - T_\ell)} \quad . \tag{7.4}$$

The value of F_{a3} must satisfy

$$0 \leq F_{a3} \leq 1 .$$

The only possible violation occurs if $h_{w\ell} < h_c$. For a given set of conditions, h_c should be the lowest heat transfer coefficient encountered for any flow regime. Since F_{a3} is applied only when $T_w \geq T_s$, then F_{a3} should always satisfy the preceding criterion. A nonzero F_{a3} will be calculated whenever $T_w > T_s$. Therefore, subcooled boiling is calculated to occur whenever $T_w > T_s$.

This form of F_{a3} also compares favorably to the following criteria: 1) F_{a3} increases as the subcooling $(T_s - T_\ell)$ decreases; 2) F_{a3} approaches unity as the liquid temperature approaches saturation; 3) F_{a3} increases as $(T_w - T_s)$ increases, and 4) To assume that all the liquid will not be evaporated less than the saturation temperature is reasonable for flow regimes for which the wall

area is proportional to the volume fraction of the liquid in accordance with the heuristic arguments in Hocevar, et al (1975). The liquid could fail this criterion for other flow regimes but no test problems have shown the criterion to be violated.

7.2 Vapor to Surface Heat Transfer - All Heat Transfer Regimes

The energy partition function for superheated condensation associated with a wall is the ratio of the amount of energy which comes from superheated condensation to the total heat transferred to the wall from the vapor:

$$F_{d4} = \frac{q_{d4}}{q_{wg}} \tag{7.6}$$

The amount of energy coming from superheated condensation, q_{d4}, is calculated as the difference between the total heat transferred to the wall and the heat convected from the vapor and is given as:

$$q_{d4} = q_{wg} - h_C \bar{A}_{wg} (T_g - T_s) \tag{7.7}$$

where h_C is the appropriate free or forced convection heat transfer coefficient for the vapor phase. The energy partition function is

$$F_{d4} = 1 - \frac{h_C \bar{A}_{wg} (T_g - T_s)}{q_{wg}} . \tag{7.8}$$

Since $q_{wg} = h_{wg} \bar{A}_{wg} (T_w - T_g)$, then F_{d4} may be expressed as

$$F_{d4} = 1 - \frac{h_C}{h_{wg}} \frac{(T_g - T_s)}{(T_g - T_w)} . \tag{7.9}$$

The value of F_{d4} will be in the range

$$0 \leq F_{d4} \leq 1$$

as long as $h_{wg} \geq h_c$ which is reasonable to expect. A nonzero F_{d4} will be calculated whenever $T_w < T_s$ and F_{d4} is calculated only when $T_w \leq T_s$. F_{d4} increases as the $T_g - T_s$ decreases. F_{d4} approaches unity as the vapor temperature approaches the saturation value. F_{d4} increases as $(T_w - T_s)$ increases. For the same reason as presented in the subcooled boiling regime, a reasonable assumption is that all vapor will not be condensed while the average vapor temperature is above the saturation temperature as long as the wall area is proportional to the volume fraction of the vapor phase.

7.3 Vapor to Liquid Heat Transfer

The energy partition functions for interphase heat transfer are computed from the heat transfer coefficients in Section 6.2. To determine the functions, the two heat transfer rates given in Section (6.2) for interphase heat transfer are considered. In all regimes two heat transfer rates were evaluated; one from the vapor to the liquid-vapor interface, q_{e7}, and the other from the interface to the liquid, q_{el}, where

$$q_{e7} = \bar{A}_{g\ell}\, h_{e7}\, (T_g - T_s) \tag{7.10}$$

$$q_{el} = \bar{A}_{g\ell}\, h_{el}\, (T_s - T_\ell). \tag{7.11}$$

In the present model a net vaporization is assumed to result if $q_{e7} > q_{el}$, while a net condensation is assumed to result if $q_{e7} < q_{el}$. The total interphase heat transfer is the largest of these two values, and is given by

$$q_{g\ell} = \text{Max}\ (q_{e7}, q_{el}) \tag{7.12}$$

The gas phase energy partition function for the interphase heat transfer, F_{e4}, is defined as the ratio of energy which comes from superheated condensation to the total interphase heat transfer. The energy which comes from superheated condensation is

$$q_{e4} = q_{g\ell} - q_{e7} \tag{7.13}$$

so that

$$F_{e4} = 1 - \frac{h_{e7} (T_g - T_s)}{\max (h_{e7} (T_g - T_s), h_{el} (T_s - T_\ell))} . \tag{7.14}$$

The value of F_{e4} will be in the range

$$0 \leq F_{e4} \leq 1$$

by definition of $q_{g\ell}$. F_{e4} is nonzero at some point when T_ℓ is below the saturation temperature. This value of T_ℓ is obtained when $q_{e7} = q_{el}$. Plots of F_{e4} are shown in Figure (7.1). These plots illustrate that F_{e4} increases as $(T_g - T_s)$ decreases. F_{e4} approaches unity as the vapor temperature approaches the saturation temperature. F_{e4} increases as $(T_s - T_\ell)$ increases. To assume that all the vapor will not be condensed at temperatures greater than the saturation temperature is reasonable for regimes for which the interphase area is proportional to the vapor volume fraction when this volume fraction is small.

The liquid phase energy partition function for the interphase heat transfer, F_{e3}, is defined as the ratio of energy which goes into subcooled boiling to the total interphase heat transfer. The energy which goes into subcooled boiling is

$$q_{e3} = q_{g\ell} - q_{el} \tag{7.15}$$

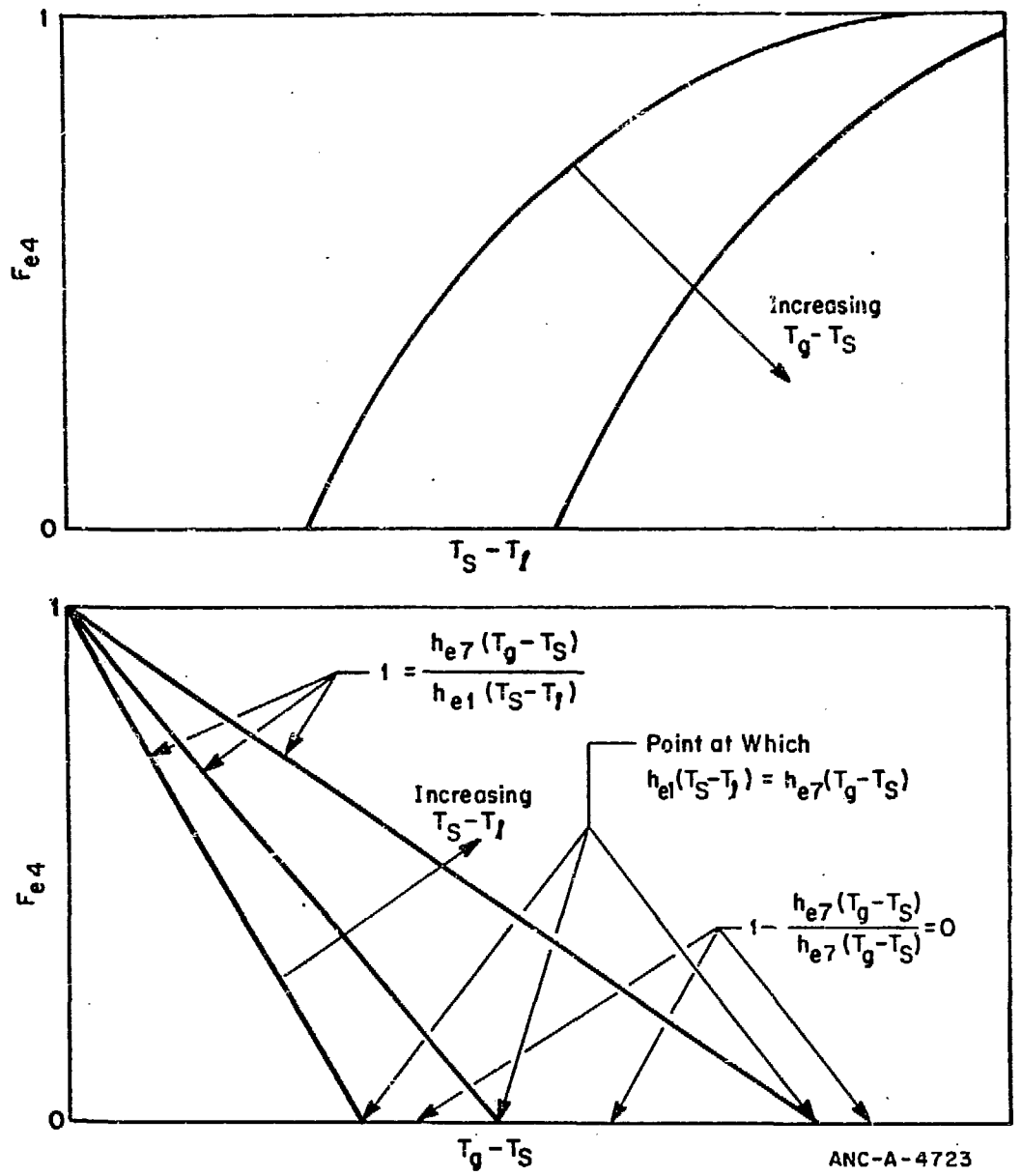

Figure 7.1 Vapor Phase Interphase Energy Distribution Function

with

$$F_{e3} = 1 - \frac{h_{el} (T_s - T_\ell)}{\max (h_{e7} (T_g - T_s), h_{el} (T_s - T_\ell))} . \qquad (7.16)$$

The value of F_{e3} will be in the range

$$0 \leq F_{e3} \leq 1$$

by definition of $q_{g\ell}$. F_{e3} is nonzero at some point when T_g is greater than the saturation temperature. This nonzero value is determined by comparison of heat transfer rates. The shape of the F_{e3} curves are the same as the F_{e4} curves with appropriate replacement of T_g, T_ℓ, and T_s. The function F_{e3} increases as $(T_s - T_\ell)$ decreases, approaches unity as the liquid temperature approaches saturation, and increases as $(T_g - T_s)$ increases. To assume that the liquid will not all be evaporated at temperatures less than the saturation temperature is reasonable for flow regimes for which the interphase area is proportional to the volume fraction of the liquid when this volume fraction is small.

A plot of the heat flux for heat transfer from a single droplet that was obtained using these interphase energy distribution functions is shown in Figure (7.2). Initially the heat transfer causes condensation of the vapor. In the course of the transient, a transition to boiling of the liquid is made.

The shape of the interphase energy partition functions presented here is similar to those presented in Hocevar, et al (1975). One important difference between the functions effects the determination of the interphase mass distribution. The mass distribution functions presented here imply that the mass at the saturation temperature due to interphase processes is either all liquid (if boiling is taking place) or all vapor (if condensation is taking place). This behavior is probably somewhat unrealistic and should be modified to include a smooth transition between these extremes.

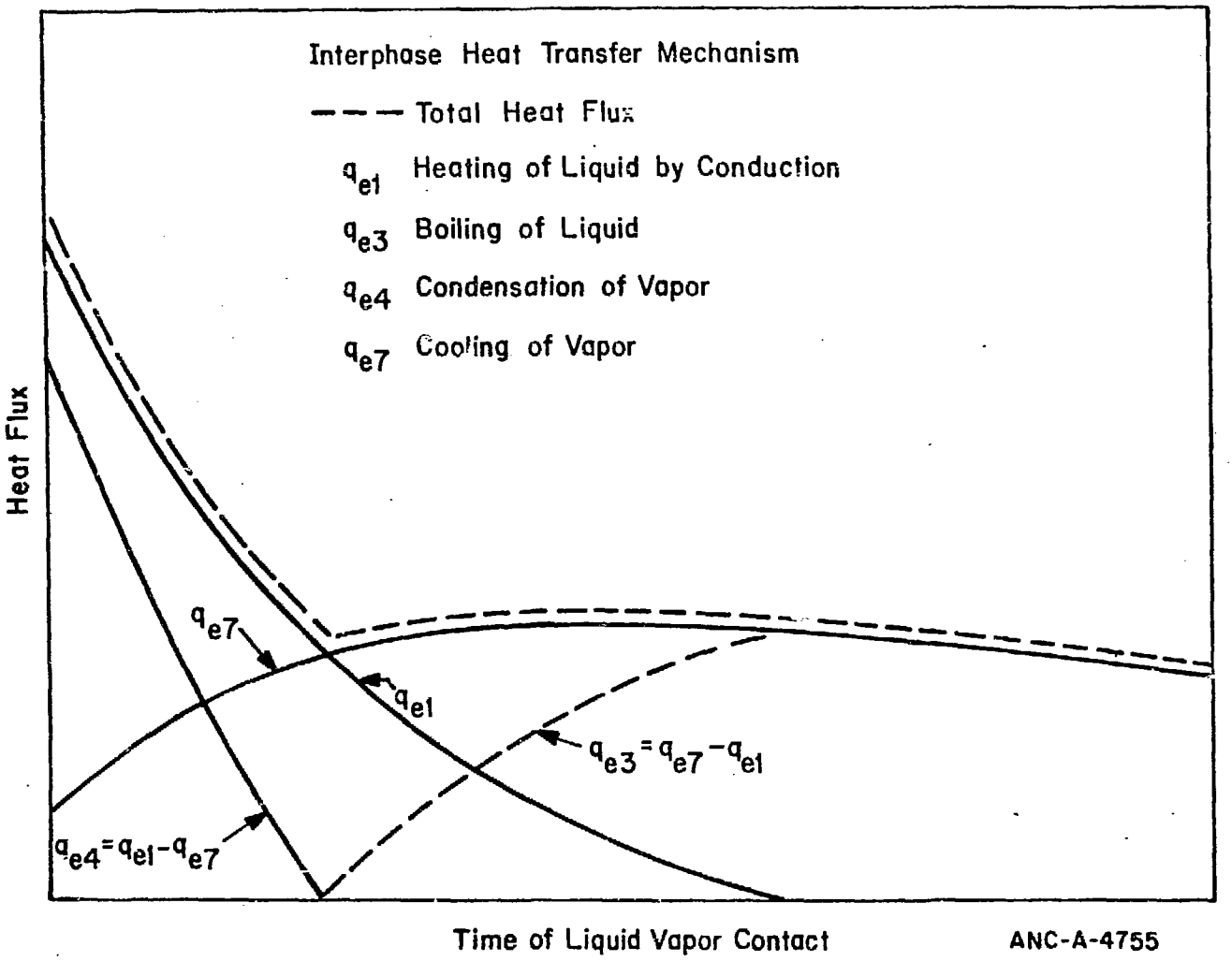

Figure 7.2 Schematic of Heat Transfer by Various Mechanisms as a Function of Time from a Single Drop

8. REFERENCES

Baker, O., 1954, "Simultaneous Flow of Oil and Gas," Oil Gas Journal, 53, p 185.

Bennett, A. W., Hewitt. G. F. Kearsey, H. A., Keevs, R. K. F., and Lacey, P. M. C., 1965, Flow Visualization Studies of Boiling at High Pressure, AERE-R 4874.

Bouré, J., Réocreux, H., Barrière, G., Flamand, J. C., and Schipfer, P., 1971, Atomic Energy Commission/Center for Nuclear Studies of Grenoble, Report TT No. 106.

Clift, R. and Gauvin W. H., 1971, "Motion of Entrained Particles in Gas Streams," Can. J. Chem. Eng., 49, p 439

Colburn, A. P., 1933, "A Method of Correlating Forced Convection Heat Transfer Data and a Comparison with Fluid Friction", Trans. Am. Inst. Chem. Engrs., 29, p 174.

Colebrook, C. F., 1938, "Turbulent Flow in Pipes with Particular Reference to the Transition Region Between the Smooth and Rough Pipe Laws," J. Inst. Civil Engs., London, Vol. II, 133.

Collier, J. G., 1972, Convective Boiling and Condensation, McGraw Hill, Limited, England.

Craine, R. F., Green, A. E. and Naghdi, P. M., 1970, Quart. Journal Mech. and Applied Math., 23, p 171.

Dittus, F. W. and Boelter, L. M. K., 1930, "Heat Transfer in Automobile Radiators of the Tubular Type" University of California, Publications in Engineering, 2, p 443.

Farman, R. F. and McFadden, J. H., 1974, "Unequal Phase Velocity Models of Annular-Dispersed Flow," Trans. Amer. Nucl. Soc., 19, p 161

Frost, C. W., and Li, K. W., 1971, "On the Rohsenow Pool-Boiling Correlation", ASMEJ. Heat Transfer, 93 c2, p 232 - 4, (May).

Fuchs, N. A., 1959, Evaporation and Droplet Growth in Gaseous Media, Pergamon, Great Britian.

Govier, G. W. and Aziz, K., 1972, The Flow of Complex Mixtures in Pipes, Van Nostrand Reinhold Co..

Green, A. E. and Naghdi, P. M., 1969, "On Basic Equations for Mixtures," Quart. Journ. Mech. and Applied Math., 22, p 427.

Hewitt, G. F., 1961, "Analysis of Annular Two-Phase Flow," Application of the Dukler Analysis to Vertical Upward Flow in a Tube, ASRE-R 3680

Harlow, F. H. and Amsden, A. A., 1975, "Numerical Calculation of Multiphase Fluid Flow," Journ. of Comp. Phys. Vol 17 pp 19-52.

Hocevar, C. J., Solbrig, C. W. and Hughes, E. D., 1975, "A Model for a Heterogeneous Two-Phase Unequal Temperature Field," (to be published).

Hsu, Y. Y., 1962, "On the Size Range of Active Nucleation Cavities on a Heating Surface", Trans. ASME, Ser C., J. Heat Transfer, 84, pp 207 - 216.

Ivey, H. J. and Morris, D. J., 1962, On the Relevance of the Vapour-Liquid Exchange Mechanism for Sub-Cooled Boiling Heat Transfer at High Pressure , AEEW - R 137.

Ivey, H. J., and Morris, 1965, "The Effect of Test Section Parameters on Saturation Pool Boiling Burnout at Atmospheric Pressure," Chem. Eng. Progr. Symposium Series 61 (60): 157 - 166.

Jacob, M., and Hawkins, G. A., 1947, Elements of Heat Transfer, John Wiley & Sons, New York.

Knudsen, J. G., and Katz, D. L., 1958, Fluid Dynamics and Heat Transfer, McGraw Hill, New York.

Kordyban, E. S. and Ranov. T., 1970, "Mechanism of Slug Formation in Horizontal Two-Phase Flow," ASME paper 70-FE-9.

Kutateladze, S. S., 1952, Heat Transfer in Condensation and Boiling , USAEC Report AEC - tr - 3770.

Marble, F. E., 1969, "Some Gasdynamic Problems in the Flow of Condensing Vapors," Astronautica Acta, 14, p 585

Mecredy, R. C. and Hamilton, L. J., 1972, "The Effects of Nonequilibruim Heat, Mass, and Momentum Transfer on Two Phase Sound Speed," Int. J. Heat Mass Transfer, 15, 61.

Merte, Jr., H., 1973, "Condensation Heat Transfer", Advances in Heat Transfer, T. F. Irvine, Jr. and J. P. Hartnett, ed, Vol. 9, pp 181 - 268.

Moalem, D. and Sideman, S., 1973, "The Effect of Motion on Bubble Collapse," Int. J. Heat Mass Transfer, 16, p 2321

Moeck, E. O., 1970, Annular-Dispersed Two-Phase Flow and Critical Heat Flux, AECL-3656.

Mugele, R. A. and Evans, H. D., 1951, "Droplet Size Distribution in Sprays," Ind. and Eng. Chemistry, 43, No. 6.

Müller, Ingo, 1968, "A Thermodynamic Theory of Mixtures of Fluids," Arch. Rational Mech. Anal., 28, 1.

Panton, Ronald, 1968, "Flow Properties for the Continuum Viewpoint of a Non-Equilibruim Gas-Particle Mixture," J. Fluid Mech., 31, 273.

Rohsenow, W. M., 1952, "A Method of Correlating Heat Transfer Data for Surface Boiling of Liquids", Trans ASME 74, p 969.

Schrock, V. E. and Grossman, L. M., 1957, "Local Heat Transfer Coefficients and Pressure Drop in Forced Convective Boiling", University of California Institute of Engineering Research Report Series 73308 - UCX 2159, No. 1, Sept. 30.

Scott, D. S., 1963, Advances in Chemical Engineering, Vol. 4, Academic Press,

Sevik, M. and Park, S. H., (1973) "The Splitting of Drops and Bubbles by Turbulent Fluid Flow", Journal of Fluids Engineering, 53.

Slattery, J. C., 1972, Momentum, Energy, and Mass Transfer in Continua, pp 182 - 184, McGraw Hill.

Snyder, N. W. and Robin, T. T., 1968, "Mass-Transfer in Subcooled Nucleate Boiling", Paper 68-HT-51, Presented at AICHE-ASME Heat Transfer Conference, Philadephia, PA., August 11-14, 1968.

Solbrig, C. W. and Hughes, E. D., 1975, "Governing Equations for a Serriated Continium: An Unequal Velocity Model for Two-Phase Flow," ANCR-1193 (April 1975).

Thom, J. R. S., Walker, W. M., Fallon, T. A. and Reising, G. F. S., 1966, "Boiling in Subcooled Water During Flow Up Heated Tubes or Annuli," Proc. Instn. Mech. Engrs., Vol. 180, Part 3C.

Tong, L. S., 1965, Boiling Heat Transfer and Two-Phase Flow, John Wiley and Sons, Inc..

Tong, L. S., 1972, Boiling Crisis and Critical Heat Flux, U. S. Atomic Energy Commission, TID - 25887.

Wallis, G. B., 1968, "Use of the Reynolds Flux Concept for Analyzing One-Dimensional Two-Phase Flow," Int. J. Heat Mass Transfer, 11, p. 445.

Wallis, G. B., 1969, One-Dimensional Two-Phase Flow, McGraw-Hill.

Yuill, W. A. and Mills, J. I., 1973, "Analytical Determination of Heat Transfer Coefficients Useful in a Loss-of-Coolant Accident Analysis," presented at Salt Lake ANS Meeting.